Accuracy of numerical simulations of contaminant transport in heterogeneous aquifers: a comparative study

F. A. Radu [a,b,*], N. Suciu [c,d], J. Hoffmann [c], A. Vogel [e],
O. Kolditz [a,f], C-H. Park [a], S. Attinger [a,b]

[a] *UFZ-Helmholtz Center for Environmental Research, Permoserstr. 15, D-04318 Leipzig, Germany*

[b] *University of Jena, Wöllnitzerstr. 7, D-07749 Jena, Germany*

[c] *Department of Mathematics, Universität Erlangen-Nürnberg, Martensstr. 3, D-91058 Erlangen, Germany*

[d] *Tiberiu Popoviciu Institute of Numerical Analysis, Romanian Academy, 400320 Cluj-Napoca, Romania*

[e] *Goethe Center for Scientific Computing,Goethe University Frankfurt, Kettenhofweg 139, D-60325 Frankfurt am Main, Germany*

[f] *Technische Universität Dresden, Helmholtzstr. 10, D-01056 Dresden, Germany*

Abstract

This work deals with a comparison of different numerical schemes for the simulation of contaminant transport in heterogeneous porous media. The numerical methods under consideration are mixed hybrid finite element (MHFEM), Galerkin finite element (GFEM), and finite volume (FVM). Concerning the GFEM we use linear and quadratic finite elements with and without upwind stabilization. Besides the classical MHFEM a new and an upwind scheme are tested. We consider higher order finite volume schemes as well as two time discretization methods: backward Euler (BE) and the second order backward differentiation formula BDF(2). It is well known that numerical (or artificial) diffusion may cause large errors. Moreover, when the Péclet number is large, a numerical code without some stabilising techniques produces oscillating solutions. Upwind schemes increase the stability but show more numerical diffusion. In this paper we quantify the numerical diffusion for the different discretization schemes and its dependency on the Péclet number. We consider an academic example and a realistic simulation of solute transport in heterogeneous aquifer. In the latter case, the stochastic estimates used as reference were obtained with global random walk (GRW) simulations, free of numerical diffusion. The results presented can be used by researchers to test their numerical schemes and stabilization techniques for simulation of contaminant transport in soil.

* Corresponding author.
   Email address: `florin.radu@ufz.de` (F. A. Radu).

1 Introduction

Environmental pollution of soils and groundwater was and remains an important problem of the world. There are hundred thousands of possible contaminated sites in western Europe alone! An active remediation of all these sites is practically (because of costs and time) impossible. Alternatively, natural attenuation has been recognized as a promising technology to restore groundwater and soil contaminated with organic pollutants because of its cost effectiveness and its potential capability of completely destroying the harmful compounds [1]. In comparison with conventionally engineered remediation technologies, natural attenuation offers a number of advantages, especially when intrinsic bioremediation is occurring [41]. Among these we mention: (a) during intrinsic bioremediation, contaminants can ultimately be transformed to innocuous by-products, not just transferred to another phase or place; (b) is less costly; (c) operate in situ. However, the decision of applying natural attenuation depends essentially on the reliable prediction of the contaminant fate and this is not an easy task [27]. Together with laboratory and field experiments, a reliable and efficient simulation tool for contaminant transport in heterogeneous soil is needed. This includes a comprehensive mathematical model, modern discretization schemes, fast nonlinear and linear solvers et cetera.

In this paper we focus on the very important problem of numerical diffusion. There is well recognized that numerical diffusion leads to erroneous solutions and therefore to false prognoses [9,20,21,23]. We propose a systematic comparative study of the numerical diffusivity of various numerical schemes, including higher order or upwind schemes. The method we use to quantify the numerical diffusion is very simple to implement and has a wide applications field. The results obtained can be used by researchers as a reference (benchmark) to test their numerical schemes or stabilization techniques.

We compare the accuracy with respect to numerical diffusion of the most popular numerical methods, e.g. GFEM, FVM and MHFEM when they are applied to advective-diffusive transport of contaminants in soil. We consider the local mass conservative MHFEM based on the lowest order Raviart-Thomas elements. Besides the classical MHFEM approach (see [11]) we propose a new, more robust MHFEM and an upwind variant of it. We continue with linear and quadratic GFEM with or without upwinding. As next, FVM, including higher orders are involved. For the temporal discretization we consider two implicit schemes: BE and BDF(2). To the best of our knowledge, a systematic comparative study of the numerical diffusivity of these methods does not exist. Here, we do this not only for an academic problem, but also for a representative, typical simulation of contaminant transport in heterogeneous soil. We formulate two tests:

T1 A problem with an analytical solution: a two-dimensional Gauss bell (Sec. 3.1). We vary the Péclet number (by changing the magnitude of water velocity and/or the diameter of the mesh) to see its influence on numerical diffusion.

T2 A realistic solute transport problem in a heterogeneous soil (Sec. 3.2). The hydraulic conductivity is stochastically generated (log-normal distributed). The wa-

ter flux is obtained by solving the flow equation.

We quantify the artificial diffusion by numerically computing the slope of the central second spatial moment of the solute concentration. In the first example (T1), we deal with a deterministic problem and it can be elementarily shown, that, for a big-enough domain, the half-slope of the second moment gives exactly the diffusion coefficient. For the second example (T2), where we conduct stochastic simulations, the half-slope of the second moment of the concentration estimates the effective diffusion coefficient (see e.g. [3,17,37]). Alternatively, the value of the effective diffusion coefficient can be theoretically obtained by homogenization or by stochastic upscaling methods (see e.g. [3]). Moreover, effective coefficients are estimated through numerical simulations with the Global Random Walk (GRW) algorithm, a superposition of a huge numbers of Particle Tracking procedures which is free of numerical diffusion and yields highly accurate results. The difference between the computed half-slope of the second moment of the solute concentration and the theoretical effective diffusion coefficient (or the one obtained by GRW simulations) gives the numerical diffusion.

The structure of this paper is as follows: after the motivation given in the introduction (Sec. 1) we present the mathematical model of contaminant transport in variable saturated porous media (Sec. 2). Also a brief description of the different numerical methods (MHFEM, GFEM, FVM, GRW) is given there. The results for the selected test examples are discussed and compared in Sec. 3 followed by the conclusions of the presented work (Sec. 4).

2 Mathematical model and discretization schemes

In this section we first present the mathematical model and then briefly summarize the used numerical methods: MHFEM (Sec. 2.2), GFEM (Sec. 2.3), FVM (Sec. 2.4) as well as the GRW method (Sec. 2.5). For more detailed descriptions see the cited literature.

2.1 Mathematical model

Let Ω be the computational domain in $\mathbb{R}^d$, $d = 1, 2$, or 3, with boundary $\partial\Omega$ and let $J = (0, T]$ be some finite interval with T denoting the final time. The diffusive-advective transport of a contaminant in soil can be mathematically described by

$$\partial_t(\Theta c) - \nabla \cdot (\mathbf{D}\nabla c - \mathbf{Q}c) = 0 \quad \text{in } J \times \Omega\,, \tag{1}$$

where $c(t, \mathbf{x})$ denotes the concentration of the contaminant and $\mathbf{D}$ is the diffusion-dispersion tensor. The water content Θ and the water flux $\mathbf{Q}$ are determinated by solving the Richards' equation, e.g. (4). Dirichlet, Neumann and/or Flux boundary conditions complete the model. For a more general model, including multicomponent reactive transport with equilibrium or non-equilibrium sorption we refer to [30].

The water flux $\mathbf{Q}(t, \mathbf{x})$ appearing in (1), as well as the water content $\Theta(\psi)$, are obtained by solving the mass balance equation for water, which is assumed incompressible

$$\partial_t\Theta(\psi) + \nabla \cdot \mathbf{Q} = 0 \tag{2}$$

and the Darcy's law

$$\mathbf{Q} = -K(\Theta(\psi))\nabla\psi, \tag{3}$$

together with initial $\psi(t = 0, \mathbf{x}) = \Psi_I(\mathbf{x})$ and boundary conditions. Above, $\psi(t, \mathbf{x})$ is the pressure head and K the hydraulic conductivity. We neglected the influence of gravity. Combining the equations (2) and (3) one obtains the Richards equation

$$\partial_t\Theta(\psi) - \nabla \cdot K(\Theta(\psi))\nabla\psi = 0 \quad \text{in } J \times \Omega\,, \tag{4}$$

which is a typical mathematical model for water flow through saturated/unsaturated soil. For the coefficient functions $\Theta(\cdot)$ and $K(\cdot)$ functional dependencies of the pressure are assumed, e.g. van Genuchten-Mualem, so that the unknowns in (2) – (3) are reduced to two. Nevertheless, in this work we consider only saturated flow, e.g. $\Theta(\psi) = \Theta_S$ and $K(\Theta(\psi)) = K_S$ are constants. We also restrict ourselves to two dimensional simulations ($d = 2$).

The following numerical schemes are presented for homogeneous Dirichlet boundary conditions for both flow and transport problems. This is just for the sake of simplicity and does not affect in any way the generality of the schemes.

4

2.2   MHFEM - mixed hybrid finite elements

We present here a classical MHFEM scheme based on the lowest order Raviart-Thomas finite elements and two new variants of it to simulate solute transport in porous media. For higher order MHFEM schemes we refer to [10]. In what follows, $L^2(\Omega)$ is the space of square integrable functions on Ω and $\langle \cdot, \cdot \rangle$ for the inner product on $L^2(\Omega)$. The functions in $H(\text{div}; \Omega)$ are vector valued, having a L^2 divergence. For the discretization in time we let $N \in \mathbb{N}$ be strictly positive, and define the time step $\tau = T/N$, as well as $t_n = n\tau$ ($n \in \{1, 2, \ldots, N\}$). Furthermore, we let $\mathcal{T}_h$ be a regular decomposition of Ω into closed d-simplices; h stands for the mesh size. We denote by $\mathcal{S}_h = \mathcal{S}_h^I \cup \mathcal{S}_h^D$ the set of all faces of $\mathcal{T}_h$, where $\mathcal{S}_h^I$ are interior faces and $\mathcal{S}_h^D$ are faces on the boundary. We always denote by $\mathbf{n}$ the outer normal. We use the discrete subspaces $W_h \subset L^2(\Omega)$ and $V_h \subset H(\text{div}; \Omega)$ defined as

$$W_h := \{p \in L^2(\Omega)| \ p \text{ is constant on each element } T \in \mathcal{T}_h\},$$

$$V_h := \{\mathbf{q} \in H(\text{div}; \Omega)| \ \mathbf{q}_{|T} = \mathbf{a} + b\mathbf{x}, \mathbf{a} \in \mathbb{R}^2, b \in \mathbb{R} \text{ for all } T \in \mathcal{T}_h\}. \tag{5}$$

In other words, W_h denotes the space of piecewise constant functions, while V_h is the lowest order Raviart-Thomas space (see [11]).

The scheme for solving the water flow (2)-(3) is based on MFEM and Euler implicit and reads

Problem 2.1 *For $n = 1, \ldots, N$ let ψ_h^{n-1} be given and find $(\psi_h^n, \mathbf{Q}_h^n) \in W_h \times V_h$ such that*

$$\langle \Theta(\psi_h^n) - \Theta(\psi_h^{n-1}), w_h \rangle + \tau \langle \nabla \cdot \mathbf{Q}_h^n, w_h \rangle = 0, \quad \forall w_h \in W_h, \tag{6}$$

$$\langle K^{-1}(\Theta(\psi_h^n))\mathbf{Q}_h^n, \mathbf{v}_h \rangle - \langle \psi_h^n, \nabla \cdot \mathbf{v}_h \rangle = 0, \quad \forall \mathbf{v}_h \in V_h. \tag{7}$$

Remark 2.1 *The problem above is still nonlinear. We solve it by a robust linearization scheme, which is first order convergent (see [26]) or by Jäger - Kačur scheme [16,15] or Newton method (see [29] for the analysis of the convergence of the Jäger - Kačur and Newton methods in the case of mixed finite elements). The solution of Problem 2.1 is obtained by hybridization (for details see [11] or below when applied to the transport equation).*

Remark 2.2 *For the convergence of the scheme for the flow Problem 2.1 we refer to [2] for strictly unsaturated flow. For saturated/unsaturated flow one can use the Kirchhoff transformation and obtain a similar scheme. That scheme is analysed in [28]. For the scheme without the Kirchhoff transformation and unsaturated/saturated flow there is no rigorous convergence result so far.*

To obtain a mixed formulation for the transport equation (1) we first introduce the flux variable $\mathbf{q}$ as additional unknown:

$$\partial_t(\Theta c) + \nabla \cdot \mathbf{q} = 0, \quad \mathbf{q} = -\mathbf{D}\nabla c + \mathbf{Q}c \quad \text{in } J \times \Omega. \tag{8}$$

The fully discrete mixed approximation of (8) now reads as follows:

Problem 2.2 *For $n = 1, \ldots, N$ let $\Theta_h^n, \Theta_h^{n-1}, \mathbf{Q_h^n}, c_h^{n-1}$ be given and find $(c_h^n, \mathbf{q_h^n}) \in W_h \times V_h$ such that there holds*

$$\langle \Theta_h^n c_h^n - \Theta_h^{n-1} c_h^{n-1}, w_h \rangle + \tau \langle \nabla \cdot \mathbf{q_h^n}, w_h \rangle = 0, \tag{9}$$

$$\langle \mathbf{D}^{-1} \mathbf{q_h^n}, \mathbf{v}_h \rangle - \langle \mathbf{D}^{-1} \mathbf{Q_h^n} c_h^n, \mathbf{v}_h \rangle - \langle c_h^n, \nabla \cdot \mathbf{v}_h \rangle = 0 \tag{10}$$

for all $w_h \in W_h$ and $\mathbf{v_h} \in V_h$.

Remark 2.3 *The convergence of the scheme is analysed in [31,32] in a very general frame, i.e. including nonlinear sorption and degradation.*

Unfortunately, the resulting equations (9)–(10) lead to a linear system of equations with an indefinite matrix such that standard iterative solvers cannot be applied. To overcome this difficulty, we use a hybridization technique (see [11]). Its basic idea is to relax firstly the continuity constraint of the normal components of the fluxes over inter-element faces that is implied by $\mathbf{v} \in H(\mathrm{div}; \Omega)$. The continuity constraint is then ensured by means of an additional variational equation involving Lagrange multipliers. Precisely, the space V_h is replaced by

$$\tilde{V}_h := \{\mathbf{q} \in L^2(\Omega) | \mathbf{q}_{|T} = \mathbf{a} + b\mathbf{x}, \mathbf{a} \in \mathrm{I\!R}^d, b \in \mathrm{I\!R} \ \text{ for all } T \in \mathcal{T}_h\}.$$

The discrete space for the Lagrange multiplier is defined by

$$\Lambda_{h,0} = \{\lambda \in L^2(\mathcal{S}_h) \mid \lambda_{|E} = \text{constant on E } \forall E \in \mathcal{S}_\mathrm{h} \text{ and } \lambda_{|E} = 0 \ \forall E \in \mathcal{S}_\mathrm{h}^\mathrm{D}\}.$$

The fully-discrete mixed hybrid variational formulation of the overall system (9)–(10) then reads as follows:

Problem 2.3 *For $n = 1, \ldots, N$ let $\Theta_h^n, \Theta_h^{n-1}, \mathbf{Q_h^n}, c_h^{n-1}$ be given and find $(c_h^n, \lambda_h^n, \mathbf{q_h^n}) \in W_h \times \Lambda_{h,0} \times \tilde{V}_h$ such that there holds*

$$\langle \Theta_h^n c_h^n - \Theta_h^{n-1} c_h^{n-1}, w_h \rangle + \tau \langle \nabla \cdot \mathbf{q_h^n}, w_h \rangle = 0, \tag{11}$$

$$\langle \mathbf{D}^{-1} \mathbf{q_h^n}, \mathbf{v}_h \rangle - \langle c_h^n, \nabla \cdot \mathbf{v}_h \rangle + \sum_{T \in \mathcal{T}_h} \langle \lambda_h^n, \mathbf{v}_h \cdot \mathbf{n} \rangle_{\partial T} = \langle \mathbf{D}^{-1} \mathbf{Q_h^n} c_h^n, \mathbf{v}_h \rangle, \tag{12}$$

$$\sum_{T \in \mathcal{T}_h} \langle \mu_h, \mathbf{q_h^n} \cdot \mathbf{n} \rangle_{\partial T} = 0 \tag{13}$$

for all $w_h \in W_h$, $\mathbf{v}_h \in \tilde{V}_h$, $\mu_h \in \Lambda_{h,0}$.

The hybridization increases first the complexity of the nonlinear systems. This drawback can be resolved by applying *static condensation* (see [11]) and eliminate now the internal degrees of freedom. Moreover, the Lagrange multipliers can be used to construct a second order accurate approximation of the primary variables [11,8]. The last observation also stays at the basis of the development of the two new schemes presented at the end of this section. The new schemes are much more robust for convection-dominated problems.

Let now Θ_T^n and c_T^n denote the water content and concentration, respectively, on the element T, $\{q_{TS}^n\}_{S \subset T}$, $\{Q_{TS}^n\}_{S \subset T}$ the components of the flux of contaminant and water, respectively, in the local Raviart-Thomas space basis $\{\mathbf{w}_{TS}\}_{S \subset T}(\mathbf{x}) = \dfrac{\mathbf{x} - \mathbf{x}_S}{d\,|T|}$ (cf. [11]), $B_{TSS'} := \displaystyle\int_T (\mathbf{D}^{-1}\mathbf{w}_{TS'}) \cdot \mathbf{w}_{TS}\, d\mathbf{x}$, and λ_S^n be the constant Lagrange multiplier on the face S. We denote by $|T| := \int_T d\mathbf{x}$ the area (volume) of element T and by $\mathbf{x}_S$ the corner of T which is not on S. We obtain from (11)–(13) the following system of nonlinear equations:

Mass conservation equation:

$$\Theta_T^n c_T^n - \Theta_T^{n-1} c_T^{n-1} + \frac{\tau}{|T|} \sum_{S \subset T} q_{TS}^n = 0 \qquad \forall\, T \in \mathcal{T}_h\,. \tag{14}$$

Equation for the flux:

$$\sum_{S' \subset T} B_{TSS'} q_{TS'}^n = \sum_{S' \subset T} B_{TSS'} Q_{TS'}^n c_T^n + c_T^n - \lambda_S^n \qquad \forall\, T \in \mathcal{T}_h, S \subset T. \tag{15}$$

Continuity of the flux over faces:

$$\sum_{T \supset S} q_{TS}^n = 0 \quad \forall\, S \in \mathcal{S}_h^I\,. \tag{16}$$

The system of equations (14)–(16) gives the **classical MHFEM scheme** (referred to as MHFEM 0 in Sec. 3) for solute transport in porous media.

A **new MHFEM scheme** is obtained by using the Lagrange multipliers, instead of the piecewise constant concentrations, for discretizing the convective term in (1). Instead of (15), this yields

$$\sum_{S' \subset T} B_{TSS'} q_{TS'}^n = \sum_{S' \subset T} B_{TSS'} Q_{TS'}^n \lambda_{S'}^n + c_T^n - \lambda_S^n \qquad \forall\, T \in \mathcal{T}_h, S \subset T. \tag{17}$$

The equations (14) and (16) remain unchanged. The **new MHFEM scheme** (referred to as MHFEM 1 in Sec. 3) is given by (14), (17) and (16). Numerical results show that the new scheme is much more robust for convection-dominated problems and has the same convergence properties as the classical scheme. A rigorous analysis of this new scheme is ongoing [33].

We also propose a **full upwind MHFEM scheme** (referred to as MHFEM 2 in Sec. 3) given by (14), (16) and

$$\sum_{S' \subset T} B_{TSS'} q_{TS'}^n = \sum_{S' \subset T} B_{TSS'} Q_{TS'}^n \alpha_{S'} + c_T^n - \lambda_S^n \qquad \forall\, T \in \mathcal{T}_h, S \subset T. \tag{18}$$

with

$$\alpha_S = \begin{cases} c_T^n, & if\ Q_{TS}^n \geq 0 \\[2mm] 2\lambda_S^n - c_T^n, & \text{otherwise} \end{cases}.$$

The upwind MHFEM scheme is suitable for highly convection-dominated-problems. The above schemes are, up to our knowledge, not reported so far in the literature.

Remark 2.4 *To obtain a discrete maximum principle, the mass matrix in (15) should be computed by a quadrature formula (cf., e.g. [24]), which has also been implemented.*

The three schemes were implemented in the *UG* toolbox (see [6]). The linear systems are solved by a multigrid method.

2.3 GFEM - Galerkin finite elements

For a description of the general case see [14] and for a more detailed description of Galerkin finite elements see e.g. [19].

For the space discretization we use the subspace $V_h^{GFEM} \subset H^1(\Omega)$

$$V_h^{GFEM} := \{v \in H^1(\Omega) | v_{|T} \in \mathcal{P}_k(T)\} \tag{19}$$

with $k = 1, 2$ where $\mathcal{P}_k(T)$ denotes the space of all polynomials up to the degree k. We restrict ourselves to Lagrange elements, i.e., all degrees of freedom are function values in fixed points. This points are called nodes. Let the nodes $\mathbf{a}_i$ $(i = 1, \ldots, M)$ be sorted such that for $i = 1, \ldots, M_1$ $\mathbf{a}_i$ is an inner node. The basis function associated with the node $\mathbf{a}_i$ is denoted by φ_i.

For the time discretization the BE method or the BDF(2) method is used, i.e., the time derivative is replaced by the difference quotient

$$D_n^{BE} u := \frac{u^n - u^{n-1}}{\tau} \quad \text{or} \quad D_n^{BDF2} u := \frac{1.5u^n - 2u^{n-1} + 0.5u^{n-2}}{\tau}. \tag{20}$$

At the first time step $(n = 1)$ the backward Euler method is applied because there is no value u^{-1}.

Differentiating out in (1) and using (2) leads to

$$\Theta \partial_t c - \nabla \cdot (\mathbf{D}\nabla c) + \mathbf{Q} \cdot \nabla c = 0. \tag{21}$$

So the fully discrete formulation of the transport problem is in case of the backward Euler method:

Problem 2.4 *Find $c_h^n \in V_h$ such that there holds*

$$\frac{\langle \Theta_h^n(c_h^n - c_h^{n-1}), v_h \rangle}{\tau} + \langle \mathbf{D}\nabla c_h^n, \nabla v_h \rangle + \langle \mathbf{Q}_h^n \cdot \nabla c_h^n, v_h \rangle = 0 \tag{22}$$

for all $v_h \in V_h^{GFEM}$.

and in case of the BDF(2) method:

Problem 2.5 *Find $c_h^1 \in V_h$ such that there holds*

$$\frac{\langle \Theta_h^1(c_h^1 - c_h^0), v_h \rangle}{\tau} + \langle \mathbf{D}\nabla c_h^1, \nabla v_h \rangle + \langle \mathbf{Q}_h^n \cdot \nabla c_h^1, v_h \rangle = 0 \qquad (23)$$

for all $v_h \in V_h^{GFEM}$ and for all $n = 2, \dots, N$ find $c_h^n \in V_h$ such that there holds

$$\frac{\langle \Theta_h^n(1.5c_h^n - 2c_h^{n-1} + 0.5c_h^{n-2}), v_h \rangle}{\tau} + \langle \mathbf{D}\nabla c_h^n, \nabla v_h \rangle + \langle \mathbf{Q}_h^n \cdot \nabla c_h^n, v_h \rangle = 0 \qquad (24)$$

for all $v_h \in V_h^{GFEM}$.

All integrals without space derivatives are assembled using mass lumping. These integrals are evaluated using a nodal quadrature formula, i.e. a quadrature rule with the quadrature points $\mathbf{a}_i$ and weights

$$\omega_i = \int_\Omega \varphi_i(\mathbf{x}) d\mathbf{x}. \qquad (25)$$

This is not possible for standard quadratic elements because some weights would be zero. Instead of that quadratic elements enriched by a bubble function (named $\overline{P}_2$) can be used (see [13]).

Let c_i^n be the concentration value in the node $\mathbf{a}_i$ at the time t_n. From (22) and (24) respectively we obtain the following system of equations

$$\omega_i \Theta_h^n(\mathbf{a}_i) D_n c_i + \int_\Omega \mathbf{D}\nabla c_h^n \cdot \nabla \varphi_i d\mathbf{x} + \int_\Omega \mathbf{Q}_h^n \cdot \nabla c_h^n \varphi_i d\mathbf{x} = 0 \quad i = 1, \dots, M_1 \qquad (26)$$

where the difference quotient D_n is D_n^{BE} in case of (22) and D_n^{BDF2} in case of (24). The integrals are evaluated with an appropriate quadrature rule.

For the convection dominated case a finite volume stabilization for linear elements is implemented. Let Ω_k denote the control volume (Donald-Diagram) associated to the node $\mathbf{a}_k$. The integral stemming from the convective term is approximated by

$$\int_\Omega \nabla \cdot (\mathbf{Q}_h^n c_h^n) \varphi_k \, d\mathbf{x} \approx \int_{\Omega_k} \nabla \cdot (\mathbf{Q}_h^n c_h^n) \, d\mathbf{x} = \int_{\partial\Omega_k} (\mathbf{Q}_h^n c_h^n) \cdot \mathbf{n} \, d\sigma. \qquad (27)$$

Another point of view is that we carry out a finite volume discretization for the whole partial differential equation. Let us consider the finite volume scheme treated in [19, chapter 6.2]. In this FV scheme, the discretization of all terms except the advective coincide with that one of the linear finite element method using mass lumping. Hence we only have to replace the advective term in the linear finite element discretization to get a finite volume scheme. The boundary integral on the right hand side of (27) can be discretized using standard finite volume techniques. We have implemented full upwinding, exponential upwinding and partial upwinding (see e.g. [19, chapter 6.2]).

The Galerkin finite elements are used only for the transport problem (1). The flow problem (2)-(3) is solved using mixed hybrid finite elements (see sec. 2.2).

The model was implemented using a software kernel for parallel computations in the field of PDEs called M++ (see [42]).

2.4 FVM - Finite Volume Method

In this section we briefly present the classical finite volume method and a generalization of the method to higher order trial spaces. In order to keep the presentation simple, we restrict ourselves to two dimensions only. However, generalizations to higher dimensions are straightforward. The classic FVM can be found in e.g. [5], a second order FVM in [22] and recently an arbitrary order FVM has been described in [39] and [40].

The FVM uses a reformulation of the equations (1) and (2). For an arbitrary control volume $B \subset \Omega$ the two equations

$$\partial_t \int_B \Theta c \, dx - \int_{\partial B} (\mathbf{D} \nabla c - \mathbf{Q} c) \cdot \mathbf{n} \, dS = 0, \tag{28}$$

$$\partial_t \int_B \Theta(\psi) \, dx - \int_{\partial B} K(\Theta(\psi)) \nabla \psi \cdot \mathbf{n} \, dS = 0. \tag{29}$$

express the conservation property of the system. In order to discretize these equations we will first choose an appropriate trial space for the unknown functions are $c(t, \mathbf{x})$ and $\psi(t, \mathbf{x})$ and then describe our choice of control volumes B.

By $\mathcal{P}_k$ we denote again the space of polynomials of degree at most k. $C^0(\Omega)$ is the space of continuous functions on Ω and we will use a trial function space for triangles defined by

$$V_h^{FVM} := \left\{ u_h \in C^0(\Omega); u_h|_T \in \mathcal{P}_p(T) \text{ for all } T \in \mathcal{T}_h \right\}. \tag{30}$$

An appropriate choice of basis functions are given by Lagrange interpolants for interpolation nodes on the triangles. Therefore, for each triangle $T \in \mathcal{T}_h$ denote its corners by $\{\mathbf{a}_0, \mathbf{a}_1, \mathbf{a}_2\}$ ($\mathbf{a}_i \in \mathbb{R}^2$) and use barycentric coordinates $(\lambda_0, \lambda_1, \lambda_2)$ in order to describe any point $\mathbf{x} \in T$, i.e., one has a representation

$$\mathbf{x} = \sum_{i=0}^2 \lambda_i(\mathbf{x}) \, \mathbf{a}_i, \quad \forall \mathbf{x} \in T. \tag{31}$$

On each triangle we have a set of $\binom{k+2}{2}$ nodes for a given degree k defined to be the points n_{i_1, i_2} of T with barycentric coordinates

$$\left(\frac{i_0}{k}, \frac{i_1}{k}, \frac{i_2}{k} \right), \quad i_0, i_1, i_2 = 0, \ldots, k, \quad i_0 + i_1 + i_2 = k. \tag{32}$$

We introduce a second decomposition $\mathcal{B}_h(\Omega) := \{B_0, B_1, B_2, \ldots\}$ of the domain Ω into (open) control volumes satisfying

$$\bigcup_i \overline{B}_i = \overline{\Omega}, \tag{33}$$

$$B_i \cap B_j = \emptyset \text{ if } i \neq j. \tag{34}$$
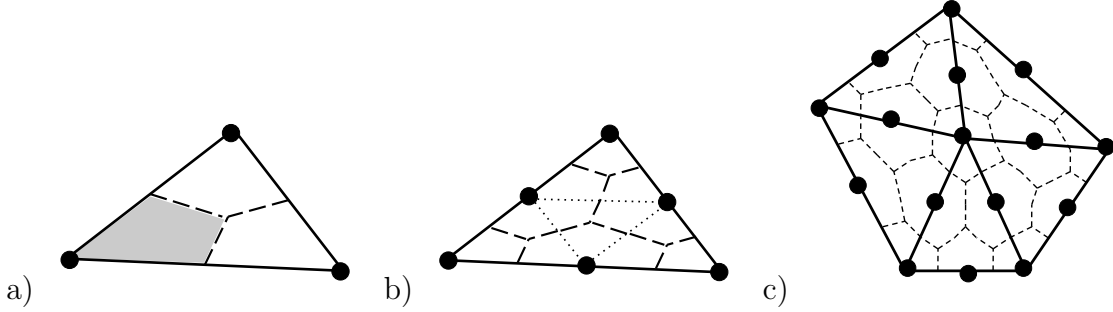
Fig. 1. Examples of control volume construction: Shown are triangles (lines), degrees of freedom (points) and control volume borders (dashed lines) and: a) linear trial space with a subcontrol volume (grey area) b) quadratic trial space with subtriangles (pointed lines) c) resulting dual decomposition for a set of triangles.

The shape of the control volume B_i will be restricted to polygons, though this is not necessary in general. Furthermore, we will construct the control volumes the way that one and only one degree of freedom of the trial space will be contained in one control volume.

In the case of a linear trial space the degrees of freedom are only located in the corners of the triangles and the control volumes can be constructed by connecting the barycenter of every triangle $T \in \mathcal{T}_h$ by straight lines with each edge midpoint. Hence, every triangle is partitioned into three parts (subcontrol volumes) and every part is associated with one node of the triangle. Now the control volume B_i containing the node i is defined by the union of all subcontrol volumes being associated with this node. A visualization is given in Fig. 1a).

For the higher order trial spaces we can reduce the construction of the control volumes to the procedure of the linear case. Indeed, we subdivide the triangles into a set of smaller subtriangles using the isolines

$$\lambda_i = \frac{j}{k}, \quad j = 1, ..., k-1, \quad i = 0, 1, 2. \tag{35}$$

On all resulting subtriangles, nodes are located in the corners only so that the structure of the subtriangles is equivalent to the structure of triangles with linear trial functions. Now we use the construction described above on these finer triangles. An example for a quadratic triangle is given in Fig. 1b) and for a set of triangles the control volumes are shown in Fig. 1c).

Now we can set up the FVM schemes using BE time stepping:

Problem 2.6 *For $n = 1, \ldots, N$ find $(c_h^n, \psi_h^n) \in V_h^{FVM} \times V_h^{FVM}$ satisfying*

$$\int_B \Theta_h^n c_h^n \, dx - \int_B \Theta_h^{n-1} c_h^{n-1} \, dx - \tau \int_{\partial B} (\mathbf{D} \nabla c_h^n - \mathbf{Q_h^n} c_h^n) \cdot \mathbf{n} \, dS = 0, \tag{36}$$

$$\int_B \Theta(\psi_h^n) \, dx - \int_B \Theta(\psi_h^{n-1}) \, dx - \tau \int_{\partial B} K(\Theta(\psi_h^n)) \nabla \psi_h^n \cdot \mathbf{n} \, dS = 0 \tag{37}$$

for all control volumes $B \in \mathcal{B}_h(\Omega)$. $\mathbf{Q_h^n} = -K(\Theta(\psi_h^n))\nabla \psi_h^n$ is the Darcy velocity and

the integrals over B and ∂B have to be replaced by appropriate quadrature rules and $\Theta_h^n = \Theta(\psi_h^n)$ for all $n \in \{0, \ldots, N\}$.

The BDF(2) time stepping scheme is obtained by replacing the time discretization D_n^{BE} with D_n^{BDF2} as described in the previous section. The FVM-schemes of arbitrary order are implemented in the UG toolbox (see [6]). In Sec. 3 we denote by FV i the FVM scheme of order i.

2.5 GRW - the global random walk algorithm

The GRW algorithm is a generalization of the particle tracking (PT) method which increases the speed of the computations and considerably improves the accuracy of the numerical simulations [38]. For a two-dimensional problem and constant porosity, the solution of a parabolic equation of form (1) is described using N particles which move in a grid, undergoing advective displacements and diffusive jumps according to the random walk law. The concentration field at a given time $t = k\delta t$ and a point $(x_1, x_2) = (i_1\delta x_1, i_2\delta x_2)$ is given by

$$c(x_1, x_2, t) = \frac{1}{N\Delta_1\Delta_2} \sum_{i_1'=-s_1}^{s_1} \sum_{i_2'=-s_2}^{s_2} n(i_1 + i_1', i_2 + i_2', k), \tag{38}$$

where $\Delta_l = 2s_l\delta x_l$, $l = 1, 2$, are the lengths of the symmetrical intervals centered at x_l and $n(i_1, i_2, k)$ is the number of particles which at time step k lie at the grid point (i_1, i_2).

The one-dimensional GRW algorithm describes the scattering of the $n(i, k)$ particles from (x_i, t_k) by

$$n(j, k) = \delta n(j, j + v_j, k) + \delta n(j + v_j - d, j, k) + \delta n(j + v_j + d, j, k),$$

where $v_j = Q_j\delta t/\delta x$ are discrete displacements produced by the velocity field and d describes the diffusive jumps. The quantities δn are Bernoulli random variables and describe respectively, the number of particles which remain at the same grid site after an advective displacement and the number of particles jumping to the left and to the right of the advected position $j + v_j$. The distribution of the particles at the next time $(k + 1)\delta t$ is given by

$$n(i, k + 1) = \sum_j \delta n(i, j, k).$$

The average number of particles undergoing diffusive jumps and the average number of particles remaining at the same node after the displacement v_j are given by the relations

$$\overline{\delta n(j + v_j \pm d, j, k)} = \frac{1}{2}r\,\overline{n(j, k)},$$

$$\overline{\delta n(j, j + v_j, k)} = (1 - r)\,\overline{n(j, k)},$$

where $0 \leq r \leq 1$. The diffusion coefficient D is related to the grid steps by the

relation

$$D = r\frac{(d\delta x)^2}{2\delta t}.$$

For two and three-dimensional cases, the same procedure is repeated for all space directions.

Because the total number of particles N contained in the grid is conserved, the GRW algorithm is stable. The condition $r \leq 1$, ensures that there is no numerical diffusion. In [38] it was shown that for Gaussian diffusion the numerical solution converges as $\mathcal{O}(\delta x^2) + \mathcal{O}(N^{-1/2})$, i.e. for large numbers of particles the convergence order is $\mathcal{O}(\delta x^2)$, the same as for the finite differences scheme.

The "reduced fluctuations" GRW algorithm is defined by

$$\delta n(j + v_j - d, j, k) = \begin{cases} n/2 & \text{if } n \text{ is even} \\ [n/2] + \theta & \text{if } n \text{ is odd} \end{cases},$$

where $n = n(j, k) - \delta n(j, j + v_j, k)$, $[n/2]$ is the integer part of $n/2$ and θ is a variable taking the values 0 and 1 with probability $1/2$. This algorithm is appropriate for large scale problems, for two reasons. Firstly, the diffusion front does not extend beyond the limit concentration defined by one particle at a grid point, keeping a physical significant shape (unlike in finite differences where a pure diffusion front has a cubic shape of side $\sim (2Dt)^{1/2}$). Secondly, the "reduced fluctuations" algorithm requires only a minimum number of calls of the random number generator.

Let us compare GRW with the classical PT scheme. PT approximates the solution of (1) by (38), after having generated (sequentially) N particles' trajectories and estimating (through a post-processing) the number of occurrences n of the N particles in sampling volumes Δ_l. PT uses N particles and T random numbers to generate a single particle trajectory. To do the same job, GRW needs a single call of the uniformly distributed random numbers generator to move all n particles from at the most as many points as the grid size L, over T time steps. Hence, (GRW-CPU time) / (PT-CPU time)=$\mathcal{O}(L/N)$. For instance, if $N = 10^{24}$ (Avogadro's number) and $L = 10^6$ grid points, a huge speed-up of computations by a factor of 10^{18} is achieved. A comparison with a PT code (diffusion over ten time steps of N particle starting at the center of a cubic grid) shows that while for the GRW algorithm there were practically no limitations concerning the total number of particles and the computation time was of about one second, PT simulations for $N = 10^9$ particles already required a computing time of about one hour and 256 processors on a CRAY T3E parallel machine [38].

To compute the variance of particle displacements, s_{ll}^2, $l = 1, 2$, a more accurate result is obtained if instead of the concentration (38) one uses the point density of the number of particles $n(i_1, i_2, k)$:

$$\frac{1}{(\delta x)^2} s_{ll}^2(k\delta t) = \frac{1}{N} \sum_{i_1, i_2} i_l^2 n(i_1, i_2, k) - \left[\frac{1}{N} \sum_{i_1, i_2} i_l\, n(i_1, i_2, k)\right]^2. \tag{39}$$

13

Using (39), the effective coefficients are computed as

$$D_{ll}^{eff}(k\delta t) = s_{ll}^2/(2k\delta t).$$

Let us consider N_{x_0} points uniformly distributed inside the initial plume, N/N_{x_0} particles at each initial point and let $n(i_1, i_2, k; i_{01}, i_{02})$ be the distribution of particles at the time step k given by the GRW procedure for a diffusion process starting at $(i_{01}\delta x_1, i_{02}\delta x_2)$. Writing the distribution for the extended plume as

$$n(i_1, i_2, k) = \sum_{i_{01},i_{02}} n(i_1, i_2, k; i_{01}, i_{02}),$$

the averages from (39) can be rewritten in the form

$$\frac{1}{N} \sum_{i_1,i_2} \alpha n(i_1, i_2, k) = \frac{1}{N_{x_0}} \sum_{i_{01},i_{02}} \left(\frac{N_{x_0}}{N} \sum_{i_1,i_2} \alpha n(i_1, i_2, k; i_{01}, i_{02}) \right), \tag{40}$$

where α stands for i_l and i_l^2 respectively. It follows from (40) that the variance (39) is an average over the trajectories of the diffusion process starting at given initial positions and over the distribution of the initial positions.

3   Numerical Investigations

This section contains the main results of the paper. We present a study to compare how diffusive the numerical schemes presented in the preceding section are. As already mentioned in the introduction we propose two tests

T1 A problem with an analytical solution: a two-dimensional Gauss bell (Sec. 3.1). We vary the Péclet number (by changing the magnitude of water velocity and, or, the diameter of the mesh) to see its influence on numerical diffusion.

T2 A realistic solute transport problem in a heterogeneous soil (Sec. 3.2). The hydraulic conductivity is stochastically generated (log-normal distributed). The water flux is obtained by solving the flow equation. A mesh with diameter $h = 0.5$ and a time step $\tau = 0.1$ are used for the computations.

In the first test (T1), we propose a deterministic problem with a known analytical solution. It can be elementarily shown that for a domain big enough, the half-slope of the central second moment of the concentration gives the diffusion coefficient. The difference between the numerically computed half-slope of the second moment and the known diffusion coefficient are then due to numerical diffusion. In the second test (T2), we conduct stochastic simulations. Now we do not have an analytical solution anymore. Nevertheless, theoretical effective diffusion coefficients can be obtained by homogenization or by stochastic upscaling methods (see e.g. [3]). On the other hand, the half-slope of the second moment is still an approximation of this effective coefficient [3,17,37]. Moreover, we are also estimating the effective diffusion coefficient by a GRW algorithm, which is known to be free of numerical diffusion. Again, the difference between the numerically computed half-slope of the second moment for MHFEM, GFEM or FVM and the theoretical diffusion coefficient or the one obtained by GRW gives the numerical diffusion.

3.1   Numerical Diffusion and Péclet Number

In this section we consider a deterministic problem with a known analytical solution. The problem represents the idealized case of solute transport without sorption or reaction in a heterogeneous soil. We quantify the numerical diffusion for the various schemes. Additionally, we study the influence of the Péclet number on numerical diffusion. Consequently, we solve the equation (1) with $\Theta = 1$ and a constant water flux $\mathbf{Q} = \begin{pmatrix} Q_x \\ Q_y \end{pmatrix}$. The computational domain is $[0, 10] \times [0, 10]$. The diffusion-dispersion coefficient is given by $\mathbf{D} = D \begin{pmatrix} 1 & 0 \\ 0 & 1 \end{pmatrix}$, with D constant. We consider adequate initial and Dirichlet boundary conditions such that equation (1) admits the analytical

solution

$$c(x,y,t) = \frac{1}{4\pi(t+\epsilon)D} e^{-\dfrac{(x-\mu_x-Q_x(t+\epsilon))^2 + (y-\mu_y-Q_y(t+\epsilon))^2}{4D(t+\epsilon)}}, \qquad (41)$$

where ϵ, μ_x, μ_y are constants. We vary the value of Q_x to investigate the dependence of the numerical diffusion on the Péclet number defined by $\text{Pe} = \dfrac{L\sqrt{Q_x^2+Q_y^2}}{D}$, with L denoting the length of the computational domain. For this we compute at each time step the first moments

$$m_x(t) = \int_{\mathbb{R}^2} xc(t,x,y)dxdy = \mu_x + v_x(t+\epsilon), \qquad (42)$$

$$m_y(t) = \int_{\mathbb{R}^2} yc(t,x,y)dxdy = \mu_y + v_y(t+\epsilon) \qquad (43)$$

and the second moments

$$m_{xx}(t) = \int_{\mathbb{R}^2} x^2 c(t,x,y)dxdy = 2D(t+\epsilon) + m_x^2. \qquad (44)$$

$$m_{yy}(t) = \int_{\mathbb{R}^2} y^2 c(t,x,y)dxdy = 2D(t+\epsilon) + m_y^2. \qquad (45)$$

As results from above, the half-slopes of the centered second moments give the diffusion coefficients:

$$D_x = \frac{1}{2}\partial_t(m_{xx} - m_x^2) = D \text{ and } D_y = \frac{1}{2}\partial_t(m_{yy} - m_y^2) = D.$$

The difference between the numerically computed half-slopes and D furnishes the numerical diffusion. The integrals are always aproximated like (this holds also for (T2))

$$\int_{\mathbb{R}^2} f(t,x,y)dxdy \approx \sum_{T\in\mathcal{T}_h} f_T(t)|T|,$$

with f_T denoting the value of f in the center of mass of T and $|T|$ stands for the area of T.

We performed simulations with $D = 0.01$, $\mu_x = \mu_y = 5$, $Q_x = 0, 0.1, 1, 2$, $Q_y = 0$ and $\epsilon = 0.1$. Accordingly, we have global Péclet numbers of 0, 100, 1000 and 2000. To see the effect of the local Péclet number ($\text{Pe}_l = h\dfrac{\sqrt{Q_x^2+Q_y^2}}{D}$) we also performed simulations on two meshes: a coarse one, with a mesh diameter $h = 0.1$ and a fine one with the mesh diameter $h = 0.05$. The time step is taken $\tau = 0.05$ and $\tau = 0.025$ for the computations on the coarse and fine mesh, respectively. The local Péclet number is for the first case 0, 1, 10, and 20, whereas for the second one 0, 0.5, 5, and 10. The results are presented in Fig. 2 – 7. The difference of D_x and

16

D_y to $D = 0.01$ divided by $D = 0.01$ gives the relative numerical diffusion. We did computations with the classical, new and upwind MHFEM schemes (see Sec. 2.2), linear, quadratic and upwind GFEM schemes (see Sec. 2.3) and first, second and third order FVM schemes (see Sec. 2.4). The numerical diffusion is very small for low Péclet numbers and obviously increases for high Péclet numbers. It can also be seen that the local Péclet number is more important than the global one, the results on a finer grid showing a clear improvement of the numerical diffusion. Nevertheless, the local Péclet number alone can not be used as a criterion for how diffusive the scheme is: the results with $Q_x = 1$ on the coarse grid are much worse than the results for $Q_x = 2$ on the fine grid, although the local Péclet numbers are identical.

The upwind schemes (MHFEM 2, partial or full upwind GFEM) should be applied only for high local Péclet numbers. These methods are stabilizing by introducing artificial diffusion [19] and this should be, if possible, avoided. We mention here that even for $Q_x = 0.1$ the full upwind schemes show artificial diffusion (like $10 - 20\%$ but because of the scale of the plot this can not be seen in the pictures Fig. 2 or Fig. 4). The partial upwind GFEM scheme is constructed in such a way that no artificial diffusion is introduced if the local Péclet number is smaller or equal to one. Nevertheless, without applying any stabilization technique the solution becomes (uncontrolled) unphysical, at extreme the solution even blows up. The results for the coarse grid and high local Péclet number are clearly showing anomalous high numerical diffusion for all discretization schemes under consideration. This comportment is due to an oscillating solution, i.e. the solution shows extremely high and/or negative values. In this case the upwind schemes furnish much better results. The results obtained with FVM are better than MHFEM or GFEM. We also mention that the upwind MHFEM scheme (MHFEM 2) is less diffusive even than the partial upwind GFEM scheme. Further, the new MHFEM scheme (MHFEM 1) is better than the classical scheme (MHFEM 0). On the finer grid, for $Q_x = 1$ the schemes without upwind are again better, i.e. the mesh is now fine enough. But for $Q_x = 2$ we still have an oscillating solution even on the fine mesh and the upwind schemes are better. If we would refine once more we will again have the schemes without upwind in advantage! Consequently, when dealing with a convection-dominated-problem we have two possibilities: we decrease the size of the discretization parameters (time step and mesh size) till the solution shows no oscilliations or apply some stabilization techniques. The first method can be very time costly, the second one may have too much numerical diffusion. The art is normally to find a compromise of the two!

The higher order schemes in space (quadratic GFEM or second or third order FVM) are showing a bit less numerical diffusion than the lower order ones on the same grid (but the number of unknowns is much higher, hence higher computational time). This is more obvious in time: BDF(2) is much less numerically diffusive than BE (see Fig. 8 and Fig. 9). We also point out that the differences are much higher in the flow direction (for D_{xx}) than in the transverse one (for D_{yy}). But the superiority of the higher order schemes is clearly seen only for 'smooth' problems like the one in (T1), for real application problems as considered in (T2), Sec. 3.2 the differences between the higher and lower order schemes are negligible (but not the differences in the computational time!).
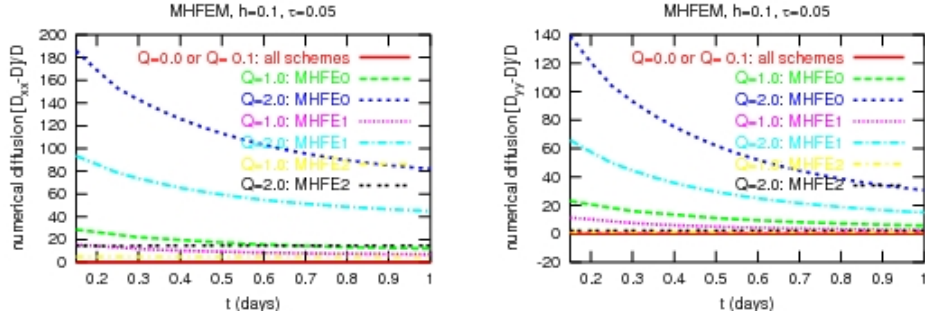
Fig. 2. Numerical diffusion for (T1): MHFEM, backward Euler. Simulations done with $h = 0.1$ and $\tau = 0.05$.
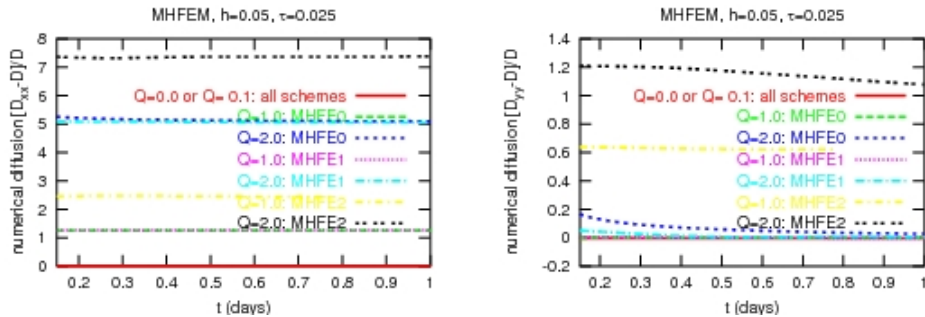

Fig. 3. Numerical diffusion for (T1): MHFEM, backward Euler. Simulations done with $h = 0.05$ and $\tau = 0.025$.
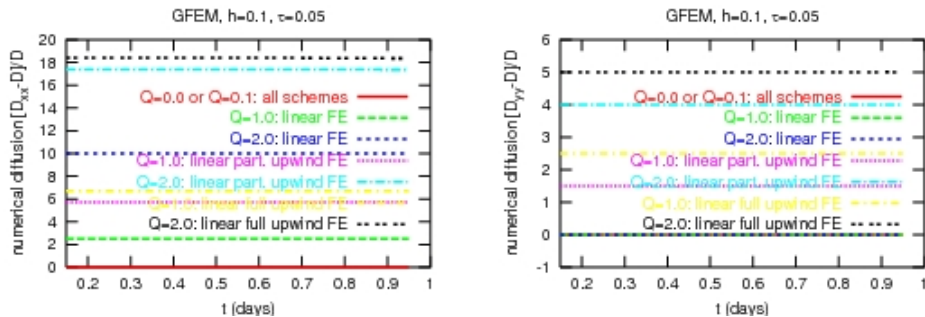

Fig. 4. Numerical diffusion for (T1): GFEM, backward Euler. Simulations done with $h = 0.1$ and $\tau = 0.05$.
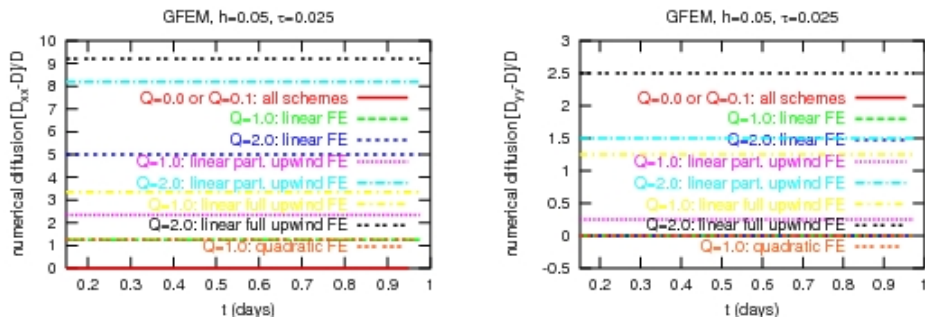

Fig. 5. Numerical diffusion for (T1): GFEM, backward Euler. Simulations done with $h = 0.05$ and $\tau = 0.025$.
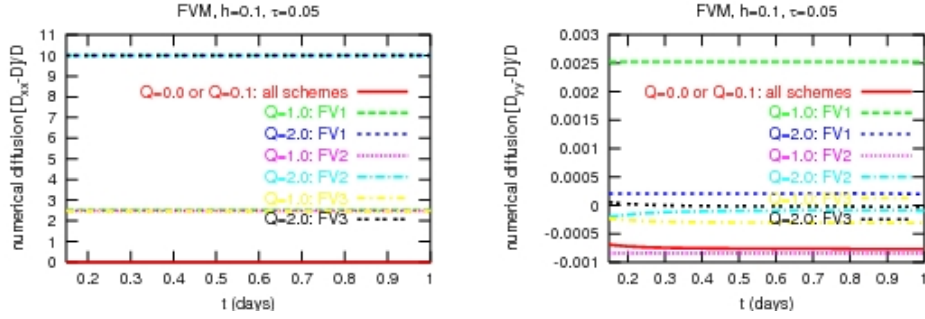
Fig. 6. Numerical diffusion for (T1): FVM, backward Euler. Simulations done with $h = 0.1$ and $\tau = 0.05$.
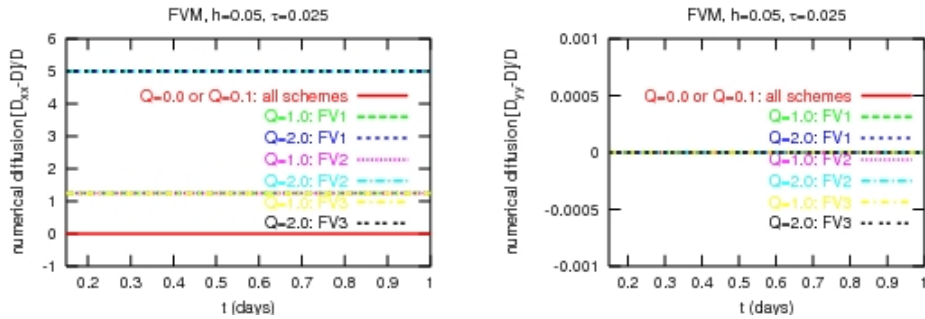
Fig. 7. Numerical diffusion for (T1): FVM, backward Euler. Simulations done with $h = 0.05$ and $\tau = 0.025$.
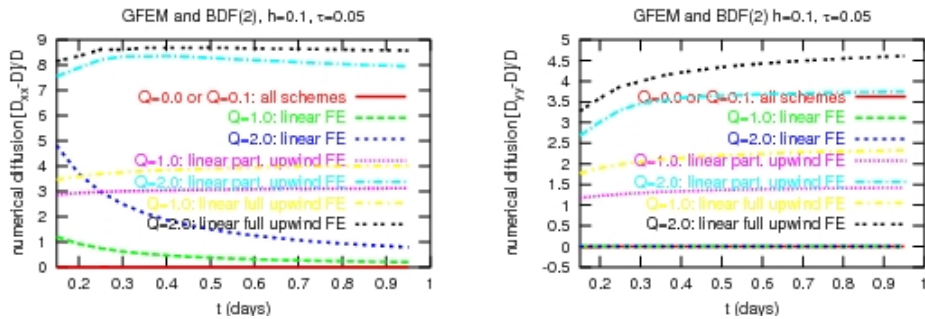
Fig. 8. Numerical diffusion for (T1): GFEM, BDF(2). Simulations done with $h = 0.1$ and $\tau = 0.05$.
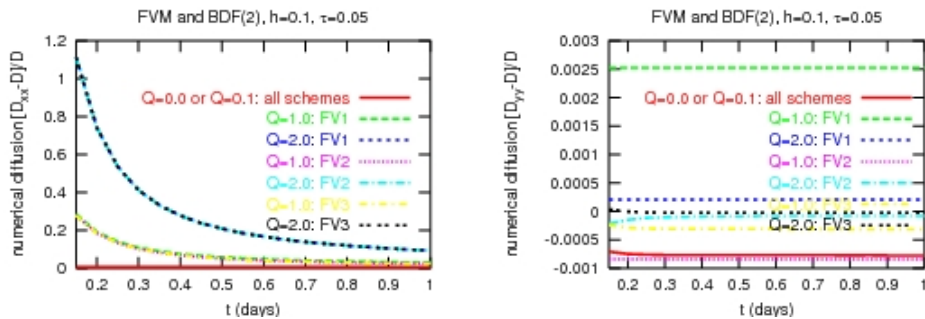
Fig. 9. Numerical diffusion for (T1): FVM, BDF(2). Simulations done with $h = 0.1$ and $\tau = 0.05$.

19

3.2 Solute transport in heterogeneous soil

In this section we study how diffusive the numerical schemes under consideration are for a realistic simulation of solute transport in heterogeneous soil. We consider here a saturated soil, i. e. $\Theta(\psi) = \Theta_S$ and $K(\Theta) = K_S$ are constants. We set $\Theta_S = 1$ and we generate a statistically normally distributed log-hydraulic conductivity as explained below. The water flux is obtained by solving (2)–(3). Let $\Omega = [0, 210] \times [0, 85]$ be the computational domain and $T = 200$ the final time. The diffusion-dispersion coefficient is given again by $\mathbf{D} = D \begin{pmatrix} 1 & 0 \\ 0 & 1 \end{pmatrix}$, with $D = 0.01$. The initial and the boundary conditions for both pressure and concentration are given in Fig. 10. The total solute mass is one. The physical units in this section are milligrams, meters and days and are not written every time explicitly.

Initial conditions

$$c_I(x, y) = \begin{cases} 0.04 & if\, (x, y) \in \Omega_I \\ 0 & otherwise \end{cases}.$$

Boundary conditions

$$\psi(x, y, t) = \begin{cases} 3.5 \; at\, x = 0 \\ 0 \quad at\, x = 210 \end{cases},$$

elsewhere
$$\mathbf{Q} \cdot \mathbf{n} = 0, \; \nabla c \cdot \mathbf{n} = 0.$$

Domain corners: (0,85), (210,85), (0,0), (210,0)

$$\Omega_I = [40, 45] \times [40, 45]$$
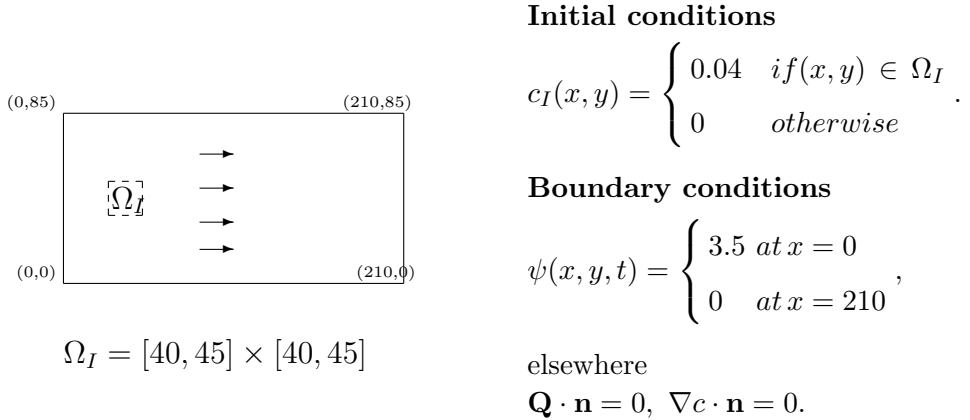
Fig. 10. Computational domain, boundary conditions, and initial conditions for (T2).

Heterogeneous aquifer systems are described by a statistically homogeneous normally distributed log-hydraulic conductivity $U(\mathbf{x}) = \log(K(\mathbf{x}))$, $\mathbf{x} \in \mathbb{R}^d$. The fluctuations random field $u(\mathbf{x}) = U(\mathbf{x}) - m$, where $m = E(U(\mathbf{x}))$ is the constant expectation of U, is homogeneous in a wide sense (or second order homogeneous) with mean zero and a correlation function which depends only on the difference vector $\boldsymbol{\rho} = \mathbf{x}_1 - \mathbf{x}_2$, i.e. $E(u(\mathbf{x}_1)u(\mathbf{x}_2)) = C(\mathbf{x}_1, \mathbf{x}_2) = C(\boldsymbol{\rho})$. To generate homogeneous random fields we used the "randomization method" [34]. The simplest variant of the randomization method has the form of a superposition of N_p random sine modes,

$$u(\mathbf{x}) = \frac{\sigma}{\sqrt{N_p}} \sum_{j=1}^{N_p} [\zeta_j \cos(2\pi\lambda\mathbf{k}_j\mathbf{x}) + \eta_j \sin(2\pi\lambda\mathbf{k}_j\mathbf{x})] , \tag{46}$$

where ζ_j, η_j, $j = 1, \ldots, N_p$ are independent Gaussian random variables of mean zero and unit variance, and $\mathbf{k}_j$ are independent random vectors. The generated random field $u(\mathbf{x})$ has the mean zero, variance σ^2, isotropic correlation described by the function $C(\rho) = \sigma^2 e^{-\rho/\lambda}$, where $\rho = \|\boldsymbol{\rho}\|$ ($\|\cdot\|$ stands for the euclidian norm) and λ is the correlation length. Fig. 11 (a) shows a sample of the random field (46) and in Fig. 11 (b) it is verified that the spatial correlation is in very good agreement with the

ensemble exponential correlation considered in the numerical setup, indicating good ergodic properties of the randomization method used in the present simulations.

For the simulations presented here we used $N_P = 6400$ modes in (46) to generate samples of log-hydraulic conductivity with $E(K_S) = 15$, $\sigma^2 = 0.1$ and $\lambda = 1$. This implies $K_g = E(K_S)e^{-\sigma^2/2} = 14.268$ (the geometrical mean gives the effective conductivity, see e.g. [4]) and therefore $E(Q_x) \approx -K_g \frac{\psi_{x=210} - \psi_{x=0}}{L} \approx 0.237$. We made 10 simulations with 10 different permeability realizations for each numerical scheme. The global Péclet number is now defined as $\text{Pe} = \frac{\lambda E(Q_x)}{D}$. We have $\text{Pe} = 23.7$. All the computations are done on a uniform grid with $h = 0.5$ and a time step $\tau = 0.1$. Fig. 12 shows the evolution of the solute plume at successive times.

The second centered moments of the concentration field were computed by

$$s_{xx} = m_{xx}(t) - m_x^2(t) = \int_\Omega x^2 c(t,x,y)dxdy - \left(\int_\Omega xc(t,x,y)dxdy \right)^2, \qquad (47)$$

$$s_{yy} = m_{yy}(t) - m_y^2(t) = \int_\Omega y^2 c(t,x,y)dxdy - \left(\int_\Omega yc(t,x,y)dxdy \right)^2. \qquad (48)$$

Using the same relations (47) - (48), with $m_\alpha(t)$, $\alpha = x,y$, replaced by their expectation $E(m_x(t)) = E(Q_x)t$ and $E(m_y(t)) = 0$ respectively, we also computed the second moments $\sigma_{\alpha\alpha}$ centered at the expected center of mass. The expectation $\Sigma_{\alpha\alpha} = E(\sigma_{\alpha\alpha})$ (estimated by the arithmetic average over the ensemble of transport simulations) gives the centered moments of the expected concentration. The latter are related to the expectation $S_{\alpha\alpha} = E(s_{\alpha\alpha})$ of the second moments of the actual concentration by

$$S_{\alpha\alpha} = \Sigma_{\alpha\alpha} - R_{\alpha\alpha},$$

where $R_{\alpha\alpha} = E\{[m_\alpha - E(m_\alpha)]^2\}$ is the variance of the center of mass [35]. For transport in velocity fields with finite correlation lengths, $R_{\alpha\alpha}$ decays to zero in the long time limit [36,37] and the half-slopes of either $S_{\alpha\alpha}$ or $\Sigma_{\alpha\alpha}$ are constant and define the numerically upscaled diffusion coefficients $D_{\alpha\alpha}^{num,*}$.

In our settings, the theoretical upscaled diffusion coefficients which describe the long-time limit Gaussian process [35] are given by

$$D^* = \begin{pmatrix} D + \overline{Q}_x\sigma^2\lambda & 0 \\ 0 & D \end{pmatrix} = \begin{pmatrix} 0.0337 & 0 \\ 0 & 0.01 \end{pmatrix},$$

with $\overline{Q}_x = E(Q_x) = 0.237$ the averaged water flux in the x-direction (on the y-direction we have $\overline{Q}_y = 0$), σ^2 the variance and λ the correlation length of the log-hydraulic conductivity field.

Fig. 13 - 15 present the mean half-slope of the central moment of the ensemble averaged concentration $\Sigma_{\alpha\alpha}$, estimated by averaging over ensembles of 10 realizations, for variants of the three methods investigated in this paper: MHFEM, GFEM, and

FVM. Further, in Fig. 17 and Fig. 18, the new MHFEM scheme (MHFEM 1), the linear GFEM scheme, and first-order FVM scheme (FV1) are compared with the results for 256 GRW simulations, done for a first-order approximation of the velocity field corresponding to random fluctuations (46) of the log-hydraulic conductivity field. The small variance of the log-hydraulic conductivity field of 0.1 considered in simulations justify the use of the first order approximations [35]. Moreover, for the small square source with edge of 5 correlation lengths, the memory effects induced by the initial conditions are negligibly small [36,37] and $\Sigma_{\alpha\alpha}$ estimates the "one-particle dispersion" which characterizes, in the mean, the pre-asymptotic transport. In these conditions, the reliable GRW estimates of $\Sigma_{\alpha\alpha}$ can serve as reference terms in these comparisons. Confidence intervals are estimated by the standard estimations of the error of the mean, given by standard deviations divided by the square root of the number of realizations. The comparison shows that, in spite of small statistical ensembles (consisting of only 10 realizations), after about 100 days the results for all the numerical schemes considered are in acceptable small ranges about the reference GRW simulations. We point out, that the MHFEM, GFEM and FVM schemes performed very similarly with respect to numerical diffusion for test (T2) (see Fig. 17 and Fig. 18). We just remark that again the upwind MHFEM scheme was better than the upwind GFEM.

As long as no upwind is performed, all the schemes show low artificial diffusion. But, also for all the schemes, the solution is oscillating (negative concentrations are observed). Although the negative concentrations are small (like 10^{-4} at most) this makes the solution unphysical. By performing upwind one clearly sees the numerical diffusion (Fig. 13 and Fig. 14). A simple 'stabilization' method is just to cut the negative concentration and put zero instead. We did this for the MHFEM and the results are obvious: the solution is now positive and the numerical diffusion remains very low (see Fig. 16). Nevertheless, such a method is normally not acceptable because one has no evidence of its asymptotic convergence. This underlines the need for alternative stabilization techniques for such problems which are not based on adding artificial diffusion.

The higher order schemes provide almost the same results as the lower order ones (see Fig. 14 and Fig. 15). But if the lower order schemes (MHFEM, GFEM and FVM) need like 6 to 8 hours for a realization on one processor, the quadratic GFEM needs about 35 hours and the FV2 almost 70 hours. And this although all the schemes are implemented in modern software packages and benefit of highly efficient linear solvers! The same holds for the BDF(2) versus BE, no significant improvement can be seen.

Finally, in Fig. 19 - 24 we plot the speed of the center of mass for the numerical schemes under consideration. The speed is given by the slope of the first moment of the concentration. On the $x-$direction the speed should be $E(Q_x) = 0.237$ and on the $y-$direction zero. All the schemes are performing very well in this respect. Nevertheless, we remark that at small times (less than 20 days) MHFEM 0 and MHFEM show relative high errors (see Fig. 19 and Fig. 20). Also the FVM schemes produce errors at small times (see Fig. 23 and Fig. 24). Only by the upwind MHFEM scheme and GFEM (see Fig. 21 and Fig. 22) the speed of the center of mass remains

from the beginning in the confidence interval. At long times, the most accurate in the x−direction was the MHFEM, whereas GFEM and FVM were better in the y−direction. We also point out that again the new MHFEM scheme (MHFEM 1) performed better as the classical one.


(a)   (b)
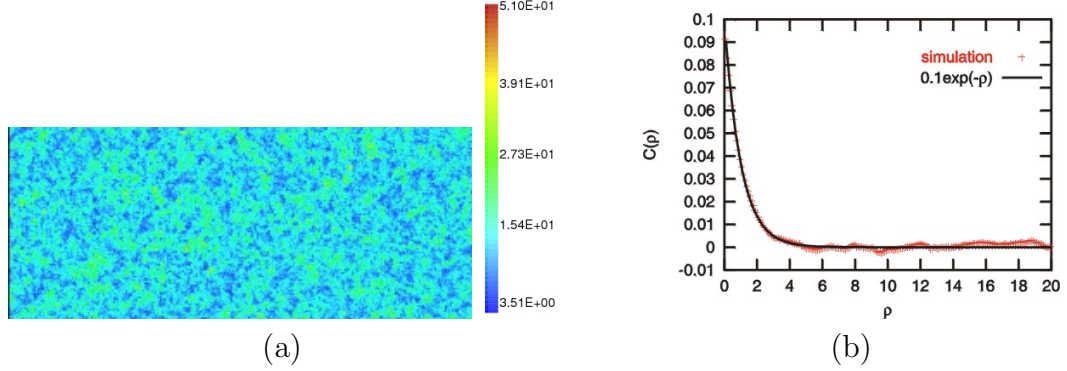
Fig. 11. (a) Sample of the random field $K = \exp U(\mathbf{x})$ generated with the uniform sampling randomization method. (b) Exponential correlation estimated by spatial averages of the random field $u(x)$ generated with the uniform samplingrandomization method.
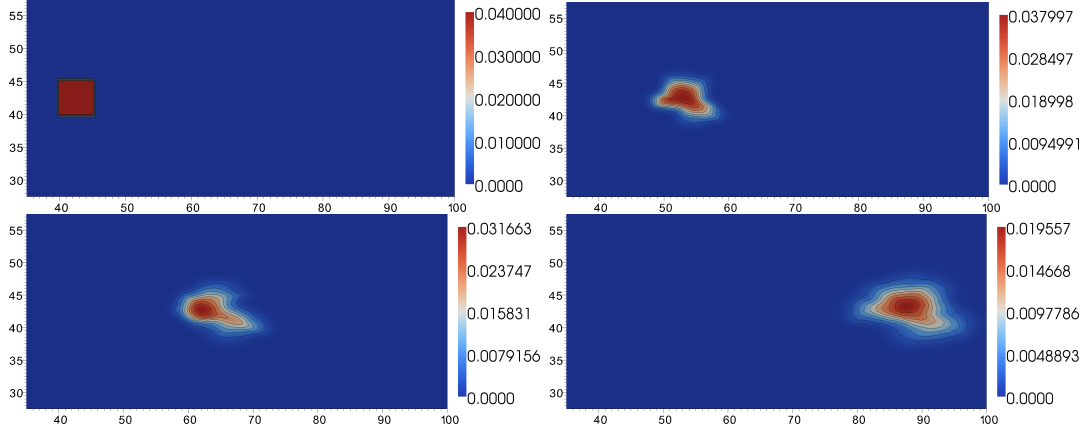
Fig. 12. Concentration profiles at 0, 50, 100 and 200 days for (T2).

23
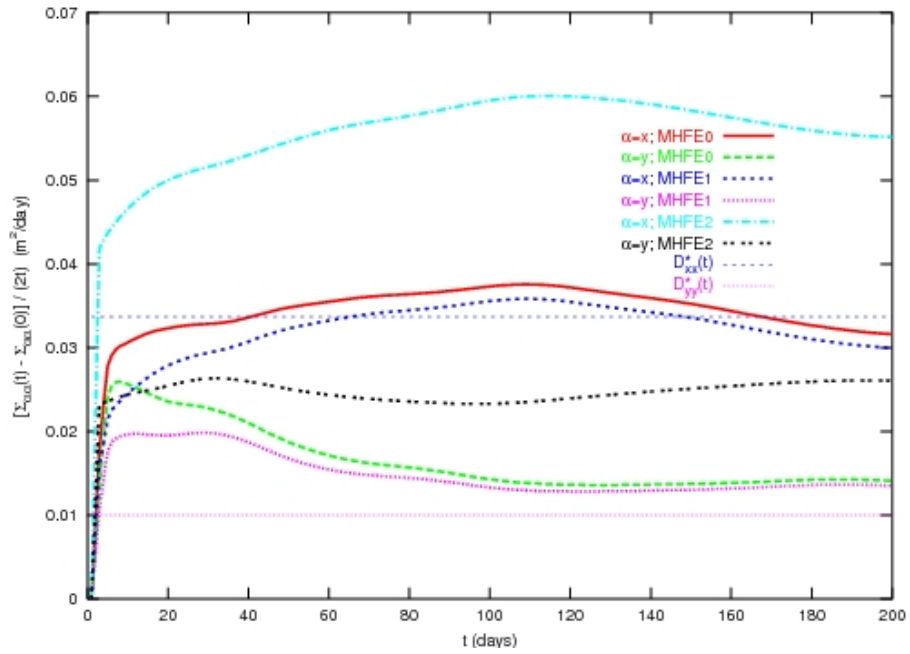
Fig. 13. Numerical diffusion for (T2) for MHFEM schemes.
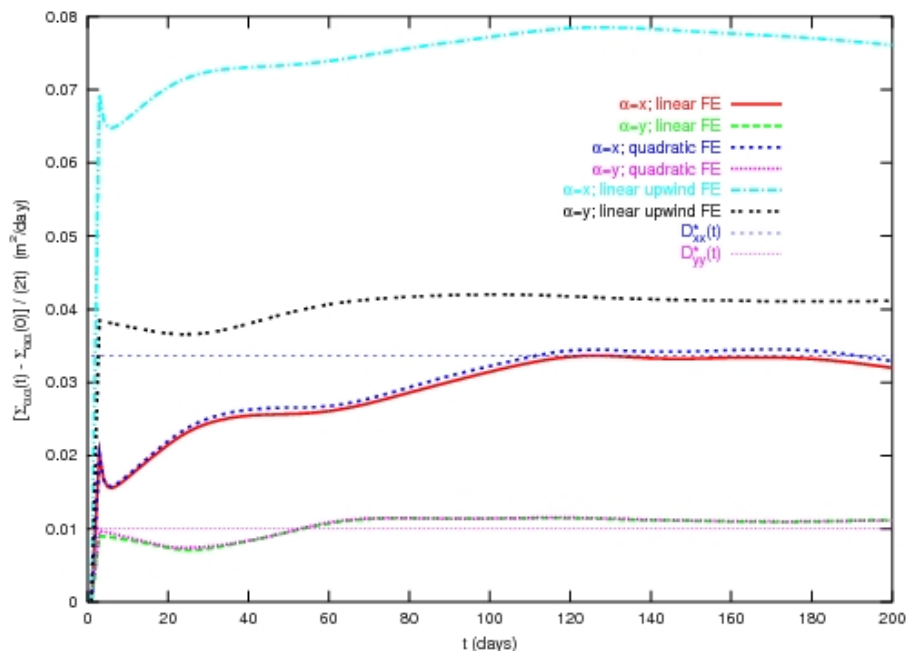
Fig. 14. Numerical diffusion for (T2) for GFEM schemes.
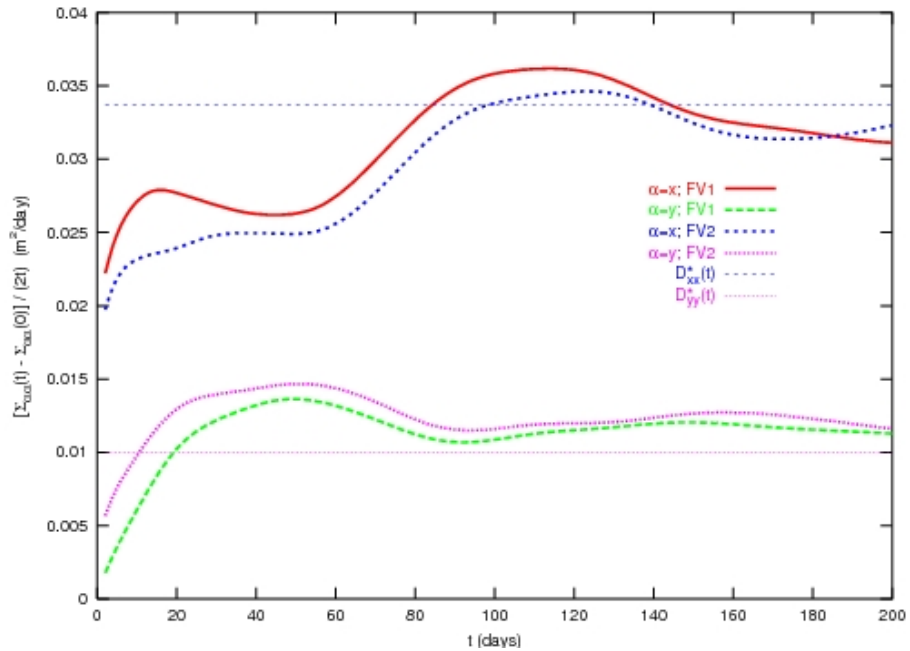
Fig. 15. Numerical diffusion for (T2) for FVM schemes.
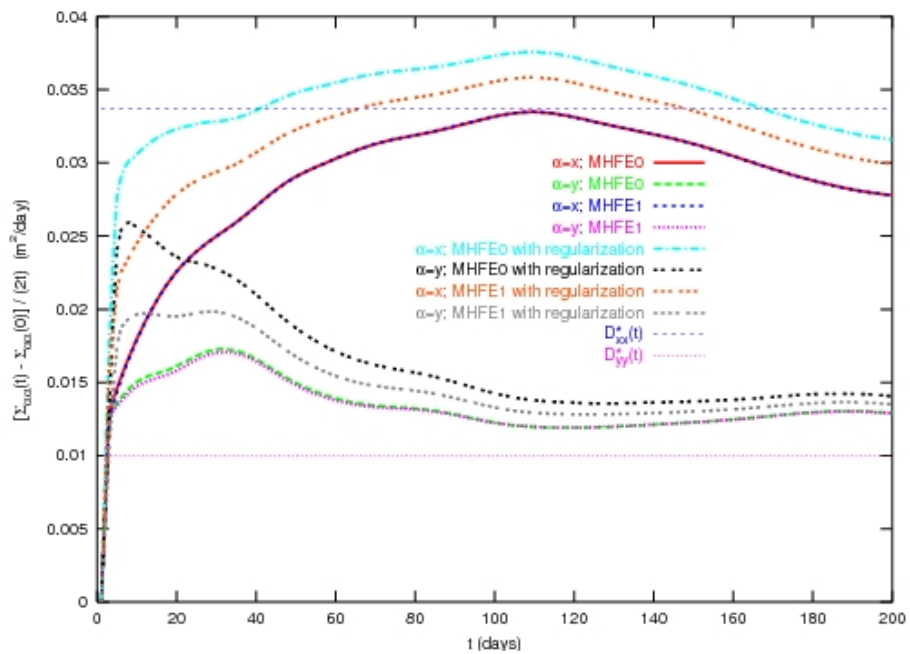
Fig. 16. Numerical diffusion for (T2) for MHFEM schemes with and without regularization.
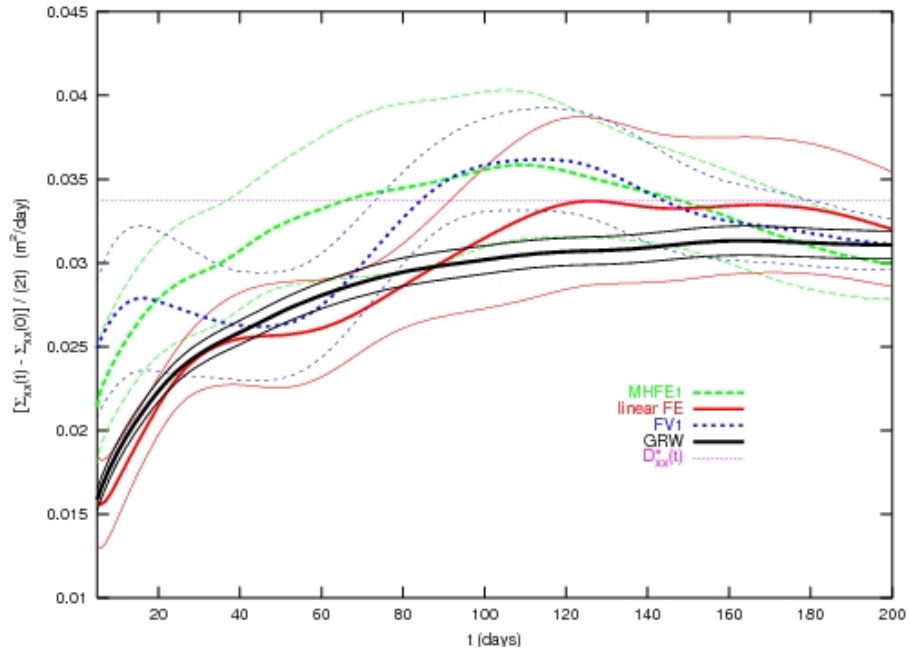
Fig. 17. Comparison of the simulated longitudinal coefficients with GRW results; thick lines represent ensemble averages and the thin lines are confidence intervals.
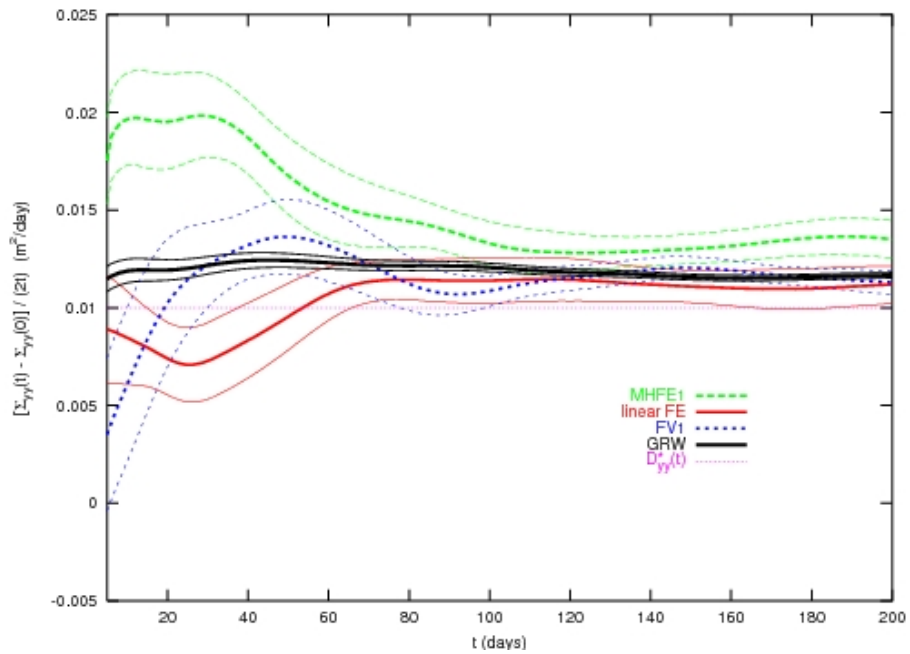

Fig. 18. Comparison of the simulated transverse coefficients with GRW results; thick lines represent ensemble averages and the thin lines are confidence intervals.
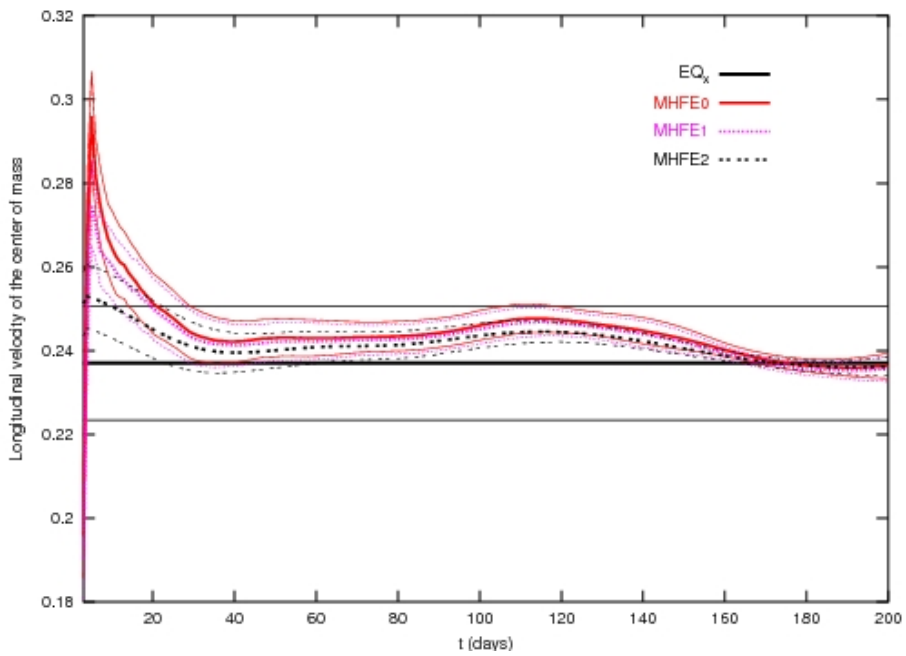
Fig. 19. Velocity (x-component) of the center of mass for MHFEM schemes; thick lines represent ensemble averages and the thin lines are confidence intervals.
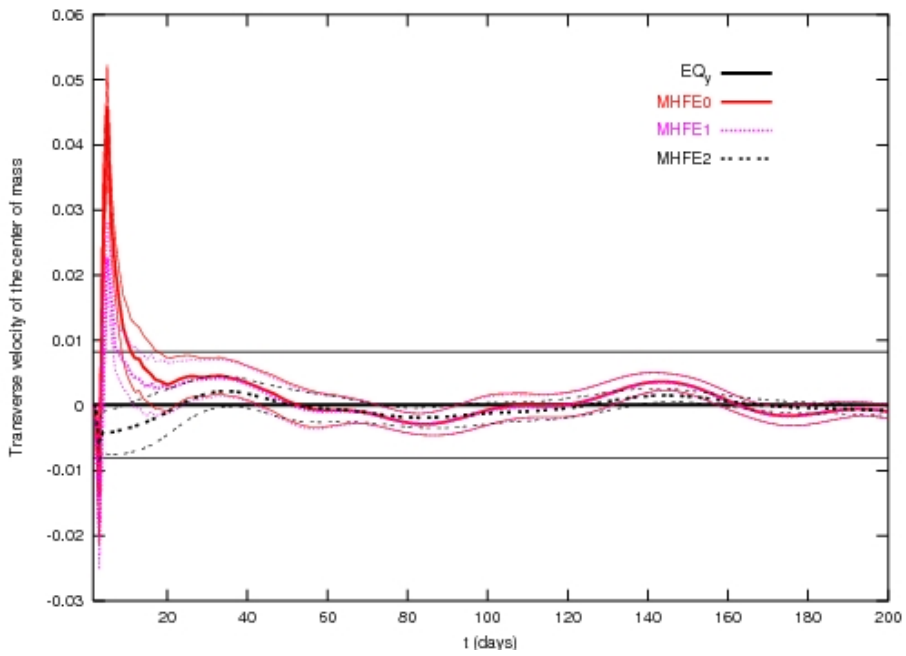

Fig. 20. Velocity (y-component) of the center of mass for MHFEM schemes; thick lines represent ensemble averages and the thin lines are confidence intervals.
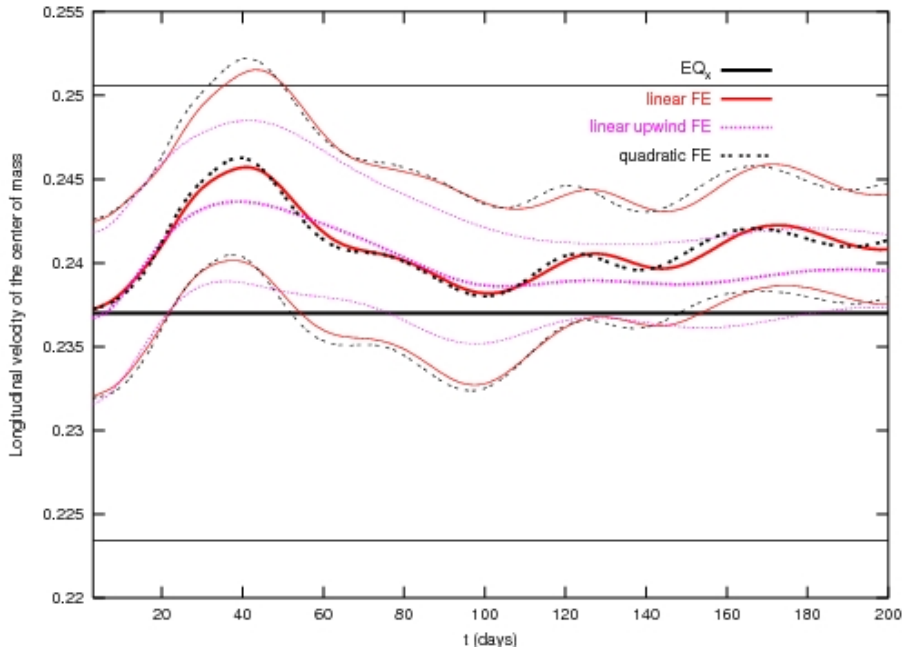
Fig. 21. Velocity (x-component) of the center of mass for GFEM schemes; thick lines represent ensemble averages and the thin lines are confidence intervals.
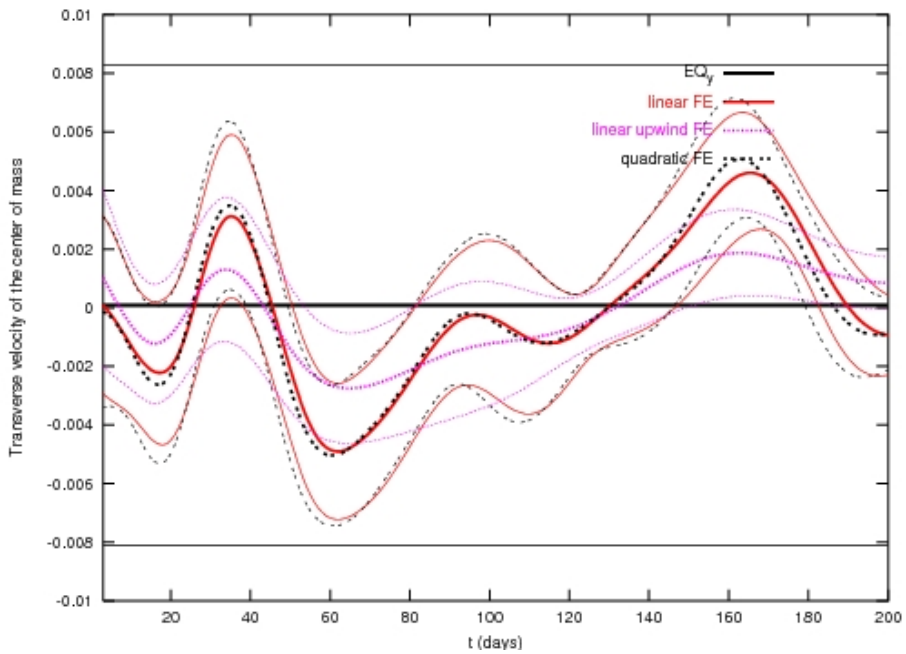

Fig. 22. Velocity (y-component) of the center of mass for GFEM schemes; thick lines represent ensemble averages and the thin lines are confidence intervals.
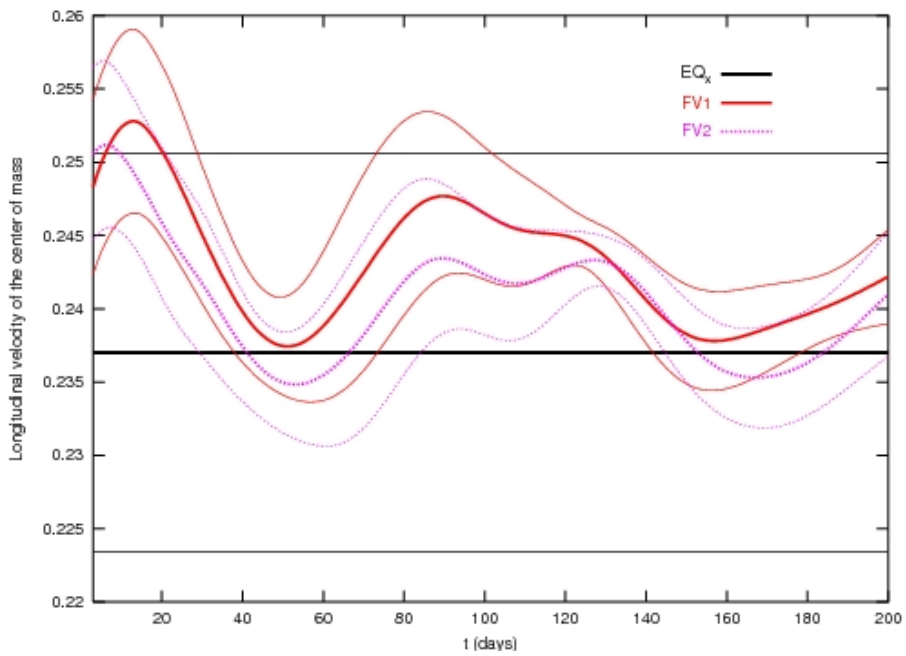
Fig. 23. Velocity (x-component) of the center of mass for FV schemes; thick lines represent ensemble averages and the thin lines are confidence intervals.
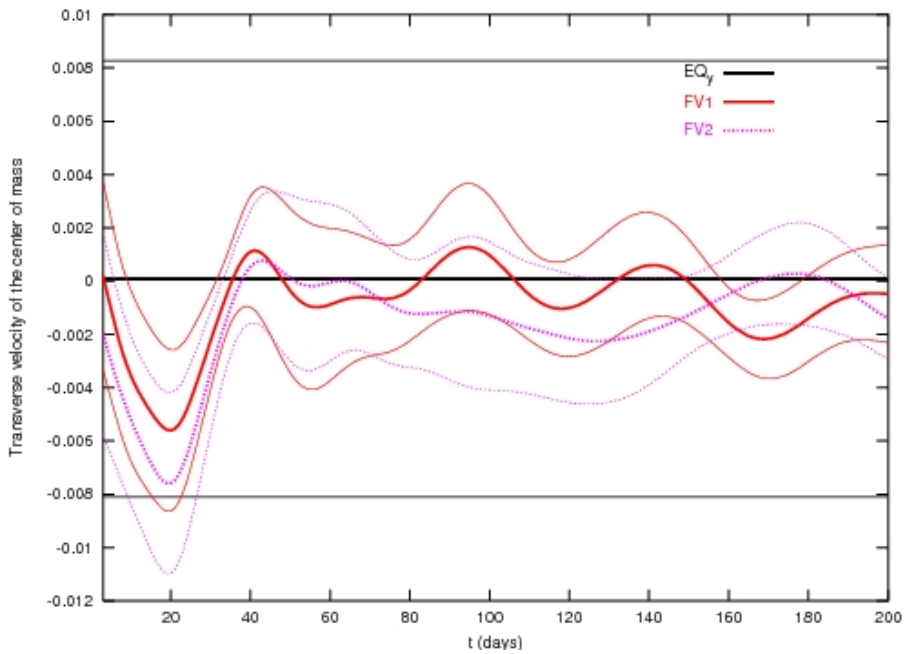

Fig. 24. Velocity (y-component) of the center of mass for FV schemes; thick lines represent ensemble averages and the thin lines are confidence intervals.

29

4   Conclusions

We considered a comparison of different numerical schemes for the simulation of contaminant transport in heterogeneous porous media. The numerical methods under consideration were Galerkin finite element (GFEM), mixed hybrid finite element (MHFEM) and finite volume (FVM). The accuracy of higher order, different time discretization methods and upwind schemes have been evaluated. We considered an academic example (where the numerical diffusion can be quantified exactly) and a realistic simulation of solute transport in heterogeneous soil. The results obtained can be used for researchers to test their numerical schemes and stabilization techniques. We summarize our findings by:

- The numerical diffusion increases with the Péclet number for all discretization schemes under consideration.
- Higher order schemes (in time or in space) show lower numerical diffusion for homogeneous problems. The cost for better accuracy is a larger computational expense. For more realistic problems (i.e. heterogeneity in parameter distribution) the differences between lower and higher order schemes are negligible but the computational cost are much higher for higher order schemes.
- Upwind schemes, on the one hand, increase the numerical stability of the transport problem, on the other hand, they introduce additional numerical diffusion. Methods without any stabilization techniques show oscillating solutions if not solved on very fine meshes and with very small time steps. Upwind schemes should only be applied when absolutely necessary. It is worthwhile to investigate and implement also other stabilization techniques.
- When dealing with a convection-dominated-problem one has two possibilities to obtain accurate solutions: (1) to decrease the size of the discretization parameters (time step and mesh diameter) till the numerical oscilliations disappear or (2) apply certain stabilization techniques. The first method can be very time costly; the second one may have too much numerical diffusion. The compromise normally is to find a balance of the two methods.
- The local Péclet number is not always (or not alone) relevant for estimating numerical diffusion. The results show that for the same local Péclet number but on different meshes and different convective fluxes the schemes are also showing different numerical diffusion (for the same type of problem).
- All the discretization under consideration are very powerfull methods and they performed very well in respect to numerical diffusion for (T2). We just mention that the FVM schemes were the most accurate for (T1) on the coarse mesh but on the fine mesh all lower order schemes without upwind gave almost the same results. The new MHFEM seems to be better than the classical one. The upwind MHFEM is less diffusive than even the partial upwind GFEM scheme. At small time steps (less than 20 days) relative high errors are observed for the speed of the center of mass for the MHFEM schemes without upwind. Also the FVM schemes produce errors at small times. Only by the upwind MHFEM scheme and GFEM the speed of the center of mass remains from the beginning in the confidence interval.

References

[1] M. ALEXANDER, *Research needs*, Environ. Sci. Technol. 25(12) (1991), pp. 1972-1973.

[2] T. ARBOGAST, M. OBEYESEKERE AND M. F. WHEELER, *Numerical methods for the simulation of flow in root-soil systems*, SIAM J. Num. Anal. 30 (1993), pp. 1677-1702.

[3] S. ATTINGER, M. DENTZ, H. KINZELBACH AND W. KINZELBACH, *Temporal behavior of a solute cloud in a chemically heterogeneous porous medium*, J. Fluid Mech. 386 (1999), pp. 77-104.

[4] S. ATTINGER, J. EBERHARD AND N. NEUSS, *Filtering procedures fo flow in heterogeneous porous media: numerical results*, Comput. Visual. Sci. 5 (2002), pp. 67-72.

[5] R. E. BANK AND D. ROSE, *Some error estimates for the box method*, SIAM Journal of Numerical Analysis 24, Issue 4 (1987), pp. 777-787.

[6] P. BASTIAN, K. BIRKEN, K. JOHANSSEN, S. LANG, N. NEUSS, H. RENTZ-REICHERT AND C. WIENERS, *UG–a flexible toolbox for solving partial differential equations*, Comput. Visual. Sci. 1 (1997), pp. 27-40.

[7] S. BAUER, C. BEYER AND O. KOLDITZ, *Assesing measurement uncertainty of first-order degradation rates in heterogenous aquifers*, Water Resources Research 42 (2006), w01420, doi:10.1029/2004WRR003878.

[8] M. BAUSE AND P. KNABNER, *Computation of variably saturated subsurface flow by adaptive mixed hybrid finite element methods*, Adv. Water Resour. 27 (2004), pp. 565-581.

[9] M. BAUSE AND P. KNABNER, *Numerical simulation of contaminant biodegradation by higher order methods and adaptive time stepping*, Comput. Visual. Sci. 7 (2004), pp. 61-78.

[10] M. BAUSE, *Higher and lowest order mixed finite element approximation of subsurface flow problems with solutions of weak regularity*, Advanced in Water Resources **31** (2007), pp. 370-382.

[11] F. BREZZI AND M. FORTIN, *Mixed and Hybrid Finite Element Methods*, Springer-Verlag, New York, 1991.

[12] H. CLASS, R. HELMIG, AND P. BASTIAN, *Numerical simulation of non-isothermal multiphase multicomponent processes in porous media. 1. An efficient solution technique*, Adv. Water Resour. 25 (2002), pp. 533-550.

[13] G. COHEN, P. JOLY, J. E. ROBERTS AND N. TORDJMAN, *Higher order triangular finite elements with mass lumping for the wave equation*, SIAM J. Numer. Anal. 38 (2001), pp. 2047-2078.

[14] J. HOFFMANN, S. KRÄUTLE AND P. KNABNER, *A Parallel Global-Implicit 2-D Solver for Reactive Transport Problems in Porous Media based on a Reduction Scheme and its Application to the MoMaS Benchmark Problem*, Computational Geosciences (2009), DOI: 10.1007/s10596-009-9173-7.

[15] W. Jäger and J. Kačur, *Solution of doubly nonlinear and degenerate parabolic problems by relaxation schemes*, M^{2}AN (Math. Model. Numer. Anal.) 29 (1995), pp. 605-627.

[16] J. Kačur, *Solution to strongly nonlinear parabolic problems by a linear approximation scheme*, IMA J. Numer. Anal. 19 (1999), 119-145.

[17] P. K. Kitanidis, *Prediction by the method of moments of transport in a heterogeneous formation*, Journal of Hydrology 102 (1988), pp. 453-473.

[18] R. Klöfkorn, D. Kröner and M. Ohlberger, *Local adaptive methods for convection dominated problems*, Internat. J. Numer. Methods in Fluids 40 (2002), pp. 79-91.

[19] P. Knabner and L. Angermann, *Numerical Methods for Elliptic and Parabolic Partial Differential Equations*, Springer, New York, 2003.

[20] R. B. Lantz, *Quantitative evaluation of numerical diffusion (truncation error)*, SPE Journal 11 (1971), pp. 315-320.

[21] R. Laval, B. R. Hodges and J. Imberger, *Reducing numerical diffusion effect with pycnocline filter*, Journal of Hydraulic Engineering 129 (2003), pp. 215-224.

[22] F. Liebau, *The finite volume element method with quadratic basis functions*, Computing 57, Issue 4 (1996), pp. 281-299.

[23] M. Ohlberger and C. Rohde, *Adaptive finite volume approximations of weakly coupled convection dominated problems*, IMA J. Numer. Anal. 22 (2002), pp. 253-280.

[24] S. Micheletti, R. Sacco and F. Saleri, *On Some Mixed Finite Element Methods with Numerical Integration*, SIAM J. Sci. Comput. 23 (2001), pp. 245-270.

[25] C-H. Park, C. Beyer, S. Bauer and O. Kolditz, *A study of preferential flow in heterogene-ous media using random walk particle tracking*, Geosciences Journal 12 (2008), pp. 205-308.

[26] I. S. Pop, F. A. Radu and P. Knabner, *Mixed finite elements for the Richards' equation: linearization procedure*, J. Comput. and Appl. Math. 168 (2004), pp. 365-373.

[27] A. Prechtel, S. Bitterlich, F. A. Radu and P. Knabner, *Natural Attenuation: hohe Anforderungen an die Modellsimulation*, Grundwasser 11 (2006), pp. 217-225.

[28] F. A. Radu, I. S. Pop and P. Knabner, *Order of convergence estimates for an Euler implicit, mixed finite element discretization of Richards' equation*, SIAM J. Numer. Anal. 42 (2004), pp. 1452-1478.

[29] F. A. Radu, I. S. Pop and P. Knabner, *On the convergence of the Newton method for the mixed finite element discretization of a class of degenerate parabolic equation*, Numerical Mathematics and Advanced Applications, A. Bermudez de Castro et al. (editors), Springer, pp. 1194-1200, 2006.

[30] F. A. Radu, M. Bause, A. Prechtel and S. Attinger, *A mixed hybrid finite element discretization scheme for reactive transport in porous media*, Numerical Mathematics and Advanced Applications, K. Kunisch, G. Of, O. Steinbach (editors), Springer, pp. 513-520, 2008.

[31] F. A. Radu, I. S. Pop and S. Attinger, *Analysis of an Euler implicit - mixed finite element scheme for reactive solute transport in porous media*, Numerical Methods Partial Differential Equations (2009), DOI:10.1002/num.20436.

[32] F. A. Radu and I. S. Pop, *Newton method for reactive solute transport with equilibrium sorption in porous media*, J. Comput. and Appl. Math. (2009), DOI:10.1016/j.cam.2009.08.070.

[33] F. A. Radu, *A more robust mixed finite element scheme for the transport equation*, in preparation.

[34] K. Sabelfeld, Monte Carlo methods in boundary value problems, Springer, Berlin, 1991.

[35] N. Suciu, C. Vamoş, J. Vanderborght, H. Hardelauf, and H. Vereecken, *Numerical investigations on ergodicity of solute transport in heterogeneous aquifers*, Water Resour. Res. 42 (2006), W04409, DOI:10.1029/2007WR004546.

[36] N. Suciu, C. Vamoş, H. Vereecken, K. Sabelfeld and P. Knabner, *Memory effects induced by dependence on initial conditions and ergodicity of transport in heterogeneous media*, Water Resour. Res. 44 (2008), W08501, DOI:10.1029/2007WR006740.

[37] N. Suciu, C. Vamoş, F. A. Radu, H. Vereecken and P. Knabner, *Persistent memory of diffusing particles*, Physical Review E 80 (2009), 061134, DOI:10.1103/PhysRevE.80.061134.

[38] C. Vamoş, N. Suciu and H. Vereecken, *Generalized random walk algorithm for the numerical modeling of complex diffusion processes*, J. Comput. Phys. 186(2) (2003), pp. 527–544.

[39] A. Vogel, *Ein Finite-Volumen-Verfahren höherer Ordnung mit Anwendung in der Biophysik (german)*, Master thesis, University of Heidelberg, 2008.

[40] A. Vogel, J. Xu, G. Wittum, *A generalization of the vertex-centered Finite-Volume scheme to arbitrary high order*, submitted to Comp. Vis. Sci. (2010).

[41] T. Wiedemeier, H. Rifai, C. Newell, J. Wilson, *Natural Attenuation of fuels and chlorinated solvents in the subsurface*, John Willey & Sons, inc., New York, 1999.

[42] C. Wieners, *Distributed point objects. A new concept for parallel finite elements.* Domain decomposition methods in science and engineering, Lecture notes in computational science and engineering, published by R. Kornhuber, R. Hoppe, J. Priaux, O. Pironneau, O. Widlund, J. Xu (editors), Springer, 2005, pp. 175-183.